



University of Kentucky
UKnowledge

Theses and Dissertations--Electrical and
Computer Engineering

Electrical and Computer Engineering

2014

MEASUREMENT AND MODELING OF HUMIDITY SENSORS

Jingbo Tong

University of Kentucky, tjbstuff@gmail.com

[Right click to open a feedback form in a new tab to let us know how this document benefits you.](#)

Recommended Citation

Tong, Jingbo, "MEASUREMENT AND MODELING OF HUMIDITY SENSORS" (2014). *Theses and Dissertations--Electrical and Computer Engineering*. 59.
https://uknowledge.uky.edu/ece_etds/59

This Master's Thesis is brought to you for free and open access by the Electrical and Computer Engineering at UKnowledge. It has been accepted for inclusion in Theses and Dissertations--Electrical and Computer Engineering by an authorized administrator of UKnowledge. For more information, please contact UKnowledge@lsv.uky.edu.

STUDENT AGREEMENT:

I represent that my thesis or dissertation and abstract are my original work. Proper attribution has been given to all outside sources. I understand that I am solely responsible for obtaining any needed copyright permissions. I have obtained needed written permission statement(s) from the owner(s) of each third-party copyrighted matter to be included in my work, allowing electronic distribution (if such use is not permitted by the fair use doctrine) which will be submitted to UKnowledge as Additional File.

I hereby grant to The University of Kentucky and its agents the irrevocable, non-exclusive, and royalty-free license to archive and make accessible my work in whole or in part in all forms of media, now or hereafter known. I agree that the document mentioned above may be made available immediately for worldwide access unless an embargo applies.

I retain all other ownership rights to the copyright of my work. I also retain the right to use in future works (such as articles or books) all or part of my work. I understand that I am free to register the copyright to my work.

REVIEW, APPROVAL AND ACCEPTANCE

The document mentioned above has been reviewed and accepted by the student's advisor, on behalf of the advisory committee, and by the Director of Graduate Studies (DGS), on behalf of the program; we verify that this is the final, approved version of the student's thesis including all changes required by the advisory committee. The undersigned agree to abide by the statements above.

Jingbo Tong, Student

Dr. Zhi D. Chen, Major Professor

Dr. Caicheng Lu, Director of Graduate Studies

MEASUREMENT AND MODELING OF HUMIDITY SENSORS

THESIS

A thesis submitted in partial fulfillment of the
requirements for the degree of Master of Science
in Electrical Engineering in the College of Engineering
at the University of Kentucky

By

Jingbo Tong

Lexington, Kentucky

Technical Director: Dr. Zhi D. Chen, Advanced Semiconductor Processing
Technology, LLC, Lexington, Kentucky

Administrative Director: Dr. Yuan Liao, Professors of Electrical Engineering,
University of Kentucky

Lexington, Kentucky

2014

Copyright © Jingbo Tong 2014

ABSTRACT OF THESIS

MEASUREMENT AND MODELING OF HUMIDITY SENSORS

Humidity measurement has been increasingly important in many industries and process control applications. This thesis research focus mainly on humidity sensor calibration and characterization. The humidity sensor instrumentation is briefly described. The testing infrastructure was designed for sensor data acquisition, in order to compensate the humidity sensor's temperature coefficient, temperature chambers using Peltier elements are used to achieve easy-controllable stable temperatures. The sensor characterization falls into a multivariate interpolation problem. Neuron networks is tried for non-linear data fitting, but in the circumstance of limited training data, an innovative algorithm was developed to utilize shape preserving polynomials in multiple planes in this kind of multivariate interpolation problems.

KEYWORDS: humidity, sensor, calibration, neuron networks, multivariate interpolation.

Jingbo Tong

November 1, 2014

MEASUREMENT AND MODELING OF HUMIDITY SENSORS

By

Jingbo Tong

Zhi D. Chen

Technical Director of Thesis

Yuan Liao

Administrative Director of Thesis

Caicheng Lu

Director of Graduate Studies

November 1, 2014

ACKNOWLEDGEMENTS

I would like to thank my advisors Dr. Zhi D. Chen and Dr. Yuan Liao for their guidance and inspiration. Dr. Chen's state of the art humidity sensor is the foundation of my further research. I also like to thank Bojie Chen for his previous work on dedicated circuitry of the humidity sensor. And my deepest gratitude goes to my parents for their support and love.

TABLE OF CONTENTS

ACKNOWLEDGEMENTS.....	iii
LIST OF TABLES.....	vi
LIST OF FIGURES	vii
Chapter 1 Introduction.....	1
1.1 Background.....	1
1.2 Problem Statement.....	3
1.3 Thesis Overview	5
Chapter 2 Basic Concepts and Definitions.....	6
2.1 Temperature and Pressure	6
2.2 Relative Humidity	7
2.3 Absolute Humidity and PPM	8
2.4 Dew Point.....	9
2.5 Dew Point Pressure Relation	10
2.6 Humidity Conversion.....	11
Chapter 3 Humidity Sensors.....	13
3.1 Relative Humidity Sensors	13
3.1.1 Polymer-Based Humidity Sensors	13
3.1.2 Ceramic Sensing Materials	15
3.1.3 Semiconducting Sensing Materials.....	17
3.2 Absolute Humidity Sensors (Hygrometers)	18
3.2.1 Chilled Mirror Hygrometer.....	18
3.2.2 Alpha-Alumina Humidity Sensor	20
Chapter 4 Dedicated Embedded System.....	27
4.1 Msp430 Architecture and Peripherals	27
4.1.1 Basic Clock Module	28
4.1.2 Timer_A3.....	30
4.1.3 Comparator_A+	34
4.2 Single Slope A/D Conversion.....	36
4.3 Temperature module.....	39
Chapter 5 Sampling System Design	43
5.1 Peltier Effect.....	44
5.2 Sampling System.....	46

Chapter 6 Experiment Results	49
Chapter 7 Temperature Compensation Modelling	57
7.1 Two Dimensional Analysis	58
7.1.1 Linear Interpolation	58
7.1.2 Polynomial Interpolation	59
7.1.3 Piecewise Cubic Interpolation	59
7.2 Three Dimensional Analysis	63
7.2.1 Artificial Neural Networks Method	63
7.2.2 3-D Delaunay Triangulation.....	67
7.2.3 An Algorithm for Sensor Temperature Compensation.....	68
7.2.4 Embedded Code Implementation	72
Chapter 8 Conclusion and Future Work	73
8.1 Conclusion	73
8.2 Future Work.....	74
REFERENCE.....	75
VITA.....	77

LIST OF TABLES

Table 1.1 Dew Point Relation to Human Comfort.....	2
Table 2.1 Molecular Weight for Some Common Gas	9
Table 2.2 Dew Point, PPM _v and Absolute Humidity Conversion.....	12
Table 4.1 Interrupt Vector Register TAIIV for Timer_A3	34
Table 6.1 Dew Point Test Points	50
Table 7.1 Modeling Points	57

LIST OF FIGURES

Figure 2.1 Saturation Vapor Pressure vs Temperature	8
Figure 2.2 Correlation Among Humidity Units	11
Figure 3.1 Two Possible Mechanisms For The “donor effect”	18
Figure 3.2 Schematic of Chilled Mirror Sensor	19
Figure 3.3 Schematic Structure of Alpha-Alumina Humidity Sensor	22
Figure 3.4 Scanning Electron Micrographs of an	23
Figure 3.5 Long Term Stability Testing Result of RH Measurement	23
Figure 3.6 Long Term Stability Testing Result of Absolute Humidity Measurement	24
Figure 3.7 Time Response Characteristics of RH variations	25
Figure 3.8 Temperature Dependence of the Sensor	26
Figure 4.1 Block Diagram of the MSP430F249 taken from datasheet.....	27
Figure 4.2 Basic Clock Module Block Diagram for MSP430F249	29
Figure 4.3 Simplified Block Diagram of the Clock Module	30
Figure 4.4 Basic Timer Block of Timer_A3	31
Figure 4.5 Block Diagram of Capture/Compare Channel 2	32
Figure 4.6 Timer_A Capture/Compare Control Register TACCTLn.....	33
Figure 4.7 Comparator_A+ Block Diagram	35
Figure 4.8 Resistance Measurement Schematic.....	37
Figure 4.9 Timing of Resistance Measurement Systems	38
Figure 4.10 Temperature Dependence of the Diode Characteristics	40
Figure 4.11 Schematic Diagram of Temperature Module.....	41
Figure 4.12 Typical SPI Timing Interface.....	42
Figure 5.1 A Calibration Laboratory of Aluminum Oxide Sensor.....	43
Figure 5.2 N-type and P-type Peltier Elements	45
Figure 5.3 A Series of Alternating N- and P-type Semiconductor Elements	45
Figure 5.4 Design of a Commercial Peltier Device	46
Figure 5.5 Illustration of Calibration Sampling System	47
Figure 6.1 Sensor Capacitance vs. Time at 30 °C.....	51
Figure 6.2 Sensor Circuit Reading vs. Time at 30 °C.....	52
Figure 6.3 Circuit Reading vs. Dew Point at 30 °C.....	53
Figure 6.4 Flaw of CS Instrument’s Humidity Sensor.....	54
Figure 6.5 Comparison of Different Dew Point/Reading Relations	55
Figure 7.1 3D Scatter Plot of Datasets.....	58
Figure 7.2 Comparison of Different interpolation Methods to an Impulse	60
Figure 7.3 Spline Vs Pchip	61
Figure 7.4 Comparison of Different Interpolants Using Dataset at 30 °C.....	62
Figure 7.5 General Structure of a Neural Network.....	64
Figure 7.6 Implemented Neural Network Diagram	65
Figure 7.7 Sample Results Using Levenberg-Marquardt Algorithm	66
Figure 7.8 Sample Results Using Bayesian Regularization Algorithm	66

Figure 7.9 Sample Results Using Bayesian Regularization Algorithm	66
Figure 7.10 Delaunay Triangulation Wired Surface of Data Points	67
Figure 7.11 Relation of Temperature and Circuit Reading at 0 °C Dew Point	69
Figure 7.12 Results after Implementing the Algorithm (1).....	71
Figure 7.13 Results after Implementing the Algorithm (2).....	71

Chapter 1 Introduction

1.1 Background

We can find humidity everywhere on earth, even in extremely dry areas, but there are cases when traces of water vapor could cause problems in some applications, and it's measurement has become increasingly important in industrial, laboratory and process control applications by allowing improvements in quality of products, reducing the cost, and increasing human comfort [1].

In the tobacco industry, properly control the humidity level can greatly improve tobacco product quality. In warehouse humidity control can protect corrosive or humidity sensitive products, such as coils of steel, food, and dried milk. One example for cost saving application is paper dryer, if we monitor the humidity in the dryer, we are able to shut down the dryer as soon as the humidity has reached a specified level. This could save a large amount of money in energy compared to the traditional way of running the dryer for a sufficient length of time to assure that the product is dry enough. There are also many examples of dew point relating to human comfort, such as humidity-controlled operating rooms, incubators, air-conditioning, and many other areas, table 1.1 from Wikipedia shows the relation between dew point and human comfort.

The humidity measurement is more difficult than that of most other properties such as pressure, temperature and flow. One of the reasons is that it covers an extremely broad measurement range, which could start from as low as 1 part-per-billion or less

(-112 °C frost point) to saturated steam at 100 °C, this covers the dynamic range of about 10⁹. Another reason is that the measurement has to be made under widely varying atmosphere. That is, under a large span of temperatures and in the presence of all kinds of contaminants, of particulate and/or chemical nature.

Table 1.1 Dew Point Relation to Human Comfort

Dew point		Human perception	Relative humidity at 32 °C (90 °F)
Over 26 °C	Over 80 °F	Severely high. Even deadly for asthma related illnesses	65% and higher
24–26 °C	75–80 °F	Extremely uncomfortable, fairly oppressive	62%
21–24 °C	70–74 °F	Very humid, quite uncomfortable	52–60%
18–21 °C	65–69 °F	Somewhat uncomfortable for most people at upper edge	44–52%
16–18 °C	60–64 °F	OK for most, but all perceive the humidity at upper edge	37–46%
13–16 °C	55–59 °F	Comfortable	38–41%
10–12 °C	50–54 °F	Very comfortable	31–37%
Under 10 °C	Under 50 °F	A bit dry for some	30%

This research is based on an alpha alumina humidity sensor, which is the world's first

drift-free humidity sensor, because the sensor is the most important part of an humidity measurement device, so a lot of work were done to test its robustness and then a more competitive product can come to reality.

1.2 Problem Statement

Sensors are bridge of the physical world and engineering world, with them we can measure almost all the physical parameters in nature. However most sensors can not be used directly, people need to use them to convert a physical quantity to an analog signal or digital data which could be read or further processed by an observer, that's where electrical circuits and microcontrollers come in. Microcontrollers are the extensively used in all kinds of intelligent instruments, it is the most important part in an embedded system which is capable of dealing with digital signals. An A/D (analog to digital) convertor is often used because microcontrollers can't process analog signal directly.

As I mentioned earlier, this thesis research is based on an alpha-alumina humidity sensor. Previous experiments using Agilent 4284A precision LCR meter to measure the sensors capacitance and resistance were conducted which shows excellent response to moisture changes. The LCR meter is big in volume, it serves as good experiment reference, but we need to have an electrical system that's dedicated for humidity measurement and the ultimate goal is by calibrating this sensor we can use it to obtain humidity data directly.

Although there are some chips on the market that are designed particularly for small

capacitance measurement, their definition doesn't meet our requirements for this sensor. And some supply high voltage on their pins, which may damage our sensor, it has a voltage limit that's lower than 5 volts. Thanks to my team member's previous work, an embedded system prototype was developed which shows very good capability of measuring capacitance, however there are still many problems remained in the circuit, one of them is it fails to give us a stable reading even when measuring an ideal capacitor. This tells us the fluctuation isn't solely come from sensor, but also from the circuit itself. So part of my research involves examining both hardware and software issues to eliminate the reading fluctuation so we can get a stable and reliable reading of the capacitance.

I need to design a sampling system which have a temperature chamber that can test the sensor under different temperatures, this alpha-alumina humidity sensor doesn't have a significant temperature drift compared to other humidity sensors, however it still need temperature compensation to obtain the best outcome.

After eliminating all problems of the hardware and software, I was able to use the improved embedded system to obtain readings of the sensor, under different temperatures in the sampling system, the readings are in non-linear relation with the capacitance of the sensor. An calibration transmitter bought from CS Instruments were used for reference, so we can know the dew point for each reading, this calibration sensor is also very important, because this is the instrument that relate our circuit reading with the dew point, a more advanced calibration instrument like chilled mirror

hygrometer is highly needed in the future.

Finally, after collecting all the experiment data, I need to develop a model which shows relation of temperature, circuit reading and dew point. Different interpolation methods and techniques will be compared for get all dew points under different temperatures and readings.

1.3 Thesis Overview

Chapter 1 has talked the importance for humidity measurement and the background for this thesis research. Chapter two will talk about the basic definitions for humidity and different humidity indication units and their conversion. Chapter 3 compares some most common types of humidity sensors and introduces the advantages of the alpha alumina humidity sensor. Chapter 4 introduces the dew point transmitter prototype that has been developed precede this research. Chapter 5 describes the calibration sampling system that has been used in this research. Chapter 6 talks about the drawback of the transmitter prototype and modifications being made to make it ready for final experiment. Chapter 7 gives the experiment set up and the results. Chapter 8 as the most important part of this thesis research discussed many methods for sensor temperature compensation, including interpolation and neural networks. Chapter 9 gives conclusion of this research and some future work that can be done to utilize and make further progress of this research result.

Chapter 2 Basic Concepts and Definitions

2.1 Temperature and Pressure

Water vapor measurements are closely related to temperature and pressure, water vapor is a form of gas, so it also follows the laws of gas. The most commonly used scale for temperature are Fahrenheit and Celsius, labeled °F and °C. In United States people use Fahrenheit while in other parts of the world people are familiar with Celsius. Both scales are linear and can be converted from each other by the following expressions:

$$^{\circ}F = 32 + 9/5^{\circ}C$$

$$^{\circ}C = ((^{\circ}F - 32))/(9/5)$$

Since water vapor exist in gas mixture, it behaves in accordance with gas laws and exerts a partial pressure in the gas mixture just like any other constituents. The ideal gas law is known as

$$PV = nRT$$

Where P is absolute pressure, V is volume, n is number of moles of gas, T is absolute temperature and R is universal gas constant. Then we have Dalton's law, this law is perhaps the most important gas law applicable to humidity measurement. Dalton supposed that if we have a mix of gases a, b, and c to be combined into a known volume at known temperature, then their individual contribution to the pressure could be written as, according to ideal gas law [2]:

$$P_a = \frac{n_a RT}{V}, P_b = \frac{n_b RT}{V}, P_c = \frac{n_c RT}{V}$$

These are he called “partial pressure” of each gas constituents. He proposed that the total pressure should be the sum of all partial pressure constituents, hence:

$$P_{total} = P_a + P_b + P_c$$

The Dalton’s law is stated as: The total pressure of a mixture of gases is equal to the sum of the pressure of the constituent gases, if each were individually to occupy that same volume, at that same temperature.

2.2 Relative Humidity

Most people are familiar with relative humidity, because they hear it on weather forecast all the time. For the relative humidity, it is the ratio of the amount of moisture in the air at a specific temperature to the maximum amount that the air could hold at that temperature, expressed as a percentage. So relative humidity is temperature dependent. More accurate definition of relative humidity is that it is the ratio of the actual partial vapor pressure to the saturation vapor pressure of the gas, multiplied with 100% at the prevailing ambient temperature. For an actual vapor pressure e , and saturation vapor pressure e_s [3],

$$Relative\ Humidity = \frac{e}{e_s} \times 100\%$$

The saturation vapor pressure with respect to water is a function of temperature and can be represented as:

$$e_s = (1.0007 + 3.46 \times 10^{-6}P)6.1121e^{17.502T/(240.97+T)}$$

The following figure shows water vapor pressure versus temperature:

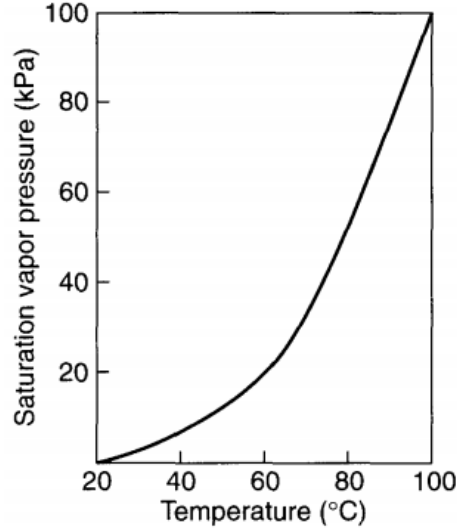


Figure 2.1 Saturation Vapor Pressure vs Temperature

2.3 Absolute Humidity and PPM

Absolute humidity is defined as water vapor density and is expressed as water mass per unit volume of dry air, it can be expressed as [4, 5]:

$$\text{Absolute humidity} = \frac{216.7e}{T_a + 273.16} \text{ (g/m}^3\text{)}$$

Where e is the vapor pressure and T_a is ambient temperature. Another absolute measurement of humidity is can be expressed as parts per million, there are two representations, one is parts per million by volume (PPM_v):

$$PPM_v = 10^6 e / (P - e)$$

Another is parts per million by weight (PPM_w), it is calculated by multiplying the above by the ratio of the molecular weight of water to that of air (if it is the carrier gas), it is given as follows:

$$PPM_w = PPM_v \times \frac{\text{Molecular Weight of Water Vapor}}{\text{Molecular Weight of Carrier Gas}}$$

For example, molecular weight of water is 18, and molecular weight of air is 29, then for air, the $PPM_w = PPM_v \times 18/29 = 0.62068966 PPM_v$. Here is a table of

molecular weight for some other gases [3]:

Table 2.1 Molecular Weight for Some Common Gas

Gas	Molecular Wt.	Gas	Molecular Wt.
Air	29	Hydrogen	2
Water	18	Ethylene	28
Acetylene	26	Helium	4
Ammonia	17	Methane	17
Argon	40	Nitrogen	28
CO ₂	44	Oxygen	32
CO	28	Sulfur Dioxide	64

2.4 Dew Point

Another important way of indicating humidity is by dew point. It is the temperature to which a volume of gas must be cooled such that it becomes saturated with respect to liquid water. This is the temperature of the above equation at a particular vapor pressure when $e = e_s$ at total pressure P [6]. The definition of frost point is very similar; it is the temperature to which a volume of gas must be cooled, such that it becomes saturated with respect to ice. From their definition, we know the units for dew and frost point are the same with temperature, but relative humidity have no unit, it is just a percentage.

Actually relative humidity only tells you how full the air is of moisture, it doesn't tell you how much moisture is in the air, nor does it tell you if there is large amount of

moisture. While people find dew point to be confusing, it is a very important variable and it is the indicator as to how much moisture is in the air. High dew points (greater than 15 °C) means that it is “sticky”, low dew points (less than -5 °C) means it is really dry. A relative humidity of 100% is an indication of dew/frost and fog, it often occurs during periods of rain. So at a very low dew point, even if the relative humidity is nearly 100%, people still feels very dry, those concepts are quite confusing. It is also important to note that the current dew point will never be higher than the current temperature and if the temperature is at the dew point and the temperature falls, the dew point must follow.

2.5 Dew Point Pressure Relation

As mentioned earlier, dew and frost point measures the partial pressure of water vapor in a gas mixture, this means there is a one-to-one relationship between vapor pressure and dew/frost point. We know from Dalton’s law that the total pressure of a gas mixture is the sum of partial pressures of all the gas constituents, so if the total pressure is raised, each partial pressure is raised in the same amount, so is water vapor pressure. This can be written as [2][7]:

$$KP_t = K(P_a + P_b + P_c + \dots + P_w)$$

Where K is a constant, P_t is total pressure, P_a , P_b , $P_c \dots$, are other gas constituents, P_w is water vapor partial pressure. Because water vapor pressure is a function of dew/frost point temperature, when the total pressure is increased, the dew/frost point increases. Likewise, when the total pressure decreases, the dew/frost point goes down,

the ratio of dew point partial pressure to the total pressure is a constant, so we have:

$$\frac{P_{w1}}{P_{t1}} = \frac{P_{w2}}{P_{t2}}$$

Where the subscripts denote different pressure cases of the same gas volume.

2.6 Humidity Conversion

We can calculate relative humidity if given temperature and dew point, likewise, we can get dew point if given temperature and relative humidity by the following equations [8]:

$$f = 100 \left(\frac{112 - 0.1T + T_D}{112 + 0.9T} \right)^8$$

$$T_D = \left(\frac{f}{100} \right)^{1/8} (112 + 0.9T) + 0.1T - 112$$

Where f , T_D , T , stands for relative humidity, dew point, temperature respectively.

We can also know temperature given dew point and relative humidity, but this is rarely the case. We often use relative humidity for higher humidity range, PPM_v are usually used for trace moisture measurement, and dew point for all range humidity indication. Both PPM_v and dew point can tell us the absolute amount of water vapor in a gas mixture. The following figure shows correlation among humidity units:

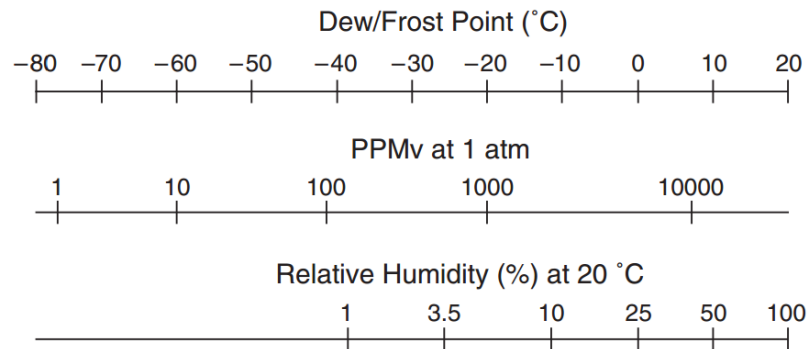


Figure 2.2 Correlation Among Humidity Units

The following is a conversion table among dew point, parts per million by volume and absolute humidity for convenience use.

Table 2.2 Dew Point, PPM_v and Absolute Humidity Conversion

DP(°C)	PPM _v	Absolute Humidity(g/m ³)	DP(°C)	PPM _v	Absolute Humidity(g/m ³)
0	6033	4.517	-50	38.89	0.02912
-2	5111	3.827	-52	30.32	0.02270
-4	4318	3.233	-54	23.51	0.01761
-6	3640	2.725	-56	18.16	0.01360
-8	3060	2.292	-58	13.96	0.01045
-10	2566	1.921	-60	10.68	0.007998
-12	2145	1606	-62	8.128	0.006087
-14	1789	1.339	-64	6.154	0.004608
-16	1487	1.113	-66	4.635	0.003471
-18	1233	0.9233	-68	3.471	0.002599
-20	1019	0.7629	-70	2.584	0.001935
-22	840	0.6291	-72	1.914	0.001433
-24	690.2	0.5169	-74	1.409	0.001055
-26	565.3	0.4233	-76	1.031	0.0007717
-28	461.3	0.3454	-78	0.7492	0.0005610
-30	375.3	0.2810	-80	0.5410	0.0004051
-32	304.1	0.2278	-82	0.3881	0.0002906
-34	245.8	0.1841	-84	0.2764	0.0002070
-36	197.8	0.1481	-86	0.1955	0.0001464
-38	158.7	0.1189	-88	0.1372	0.0001028
-40	126.8	0.09491	-90	0.09564	0.00007161
-42	100.9	0.07555	-92	0.06611	0.00004950
-44	80.03	0.05993	-94	0.0452	0.00003394
-46	63.19	0.04732	-96	0.03087	0.00002308
-48	49.67	0.03720	-98	0.02077	0.00001555
			-100	0.01387	0.00001039

Chapter 3 Humidity Sensors

According to the measurement unit, humidity sensors can be divided into two types: Relative humidity (RH) sensors and absolute humidity (trace moisture) sensors. Most humidity sensors are Relative humidity sensors which can then be divided into three categories: polymer, ceramic, and semiconductor humidity sensors. Two types of absolute humidity sensors or hygrometers are often being used: chilled-mirror hygrometer and aluminum oxide humidity sensor [9].

Relative humidity sensors offers relatively low definition and sensitivity, that's why they are used for relative humidity measurement, which is suitable for higher humidity indication, at trace humidity levels, relative humidity is rather meaningless since the total amount of moisture is too low to be described evenly from 1% to 100%. Absolute humidity, on the other hand, with high sensitivity and accuracy provided, can be used for both relative and absolute humidity measurements. This chapter will talk RH sensors briefly first and then introduces absolute humidity sensors and hygrometer, the alpha-alumina humidity sensor being used in this thesis research is emphasized. The major problem in Aluminum Oxide sensors, long-term instability has been solved. The alpha alumina sensors may have promising future in industry.

3.1 Relative Humidity Sensors

3.1.1 Polymer-Based Humidity Sensors

Organic polymers are macromolecules in which a unit structure repeats. Most of the polymers are carbon-hydride compounds or their derivatives. The carbon atoms link

each other one by one, either by sigma bond (single bond) or sigma bond plus pi bond (double bonds or triple bonds), forming a long chain, which is called the backbone of the polymer. Functional groups are rooted on the backbone, which could be either single atoms or molecular groups. The functional groups, along with the basic structure of the backbone, determine the chemical and physical properties of the polymers [10]. Artificial polymers are synthesized from monomers that are small molecules. Copolymers are polymers synthesized from two or more different kinds of monomers. Polymeric humidity sensors have been widely studied in research and applied in industry for more than 30 years. Most of the sensors are based on porous polymer films thinner than millimeters and their sensing principle is quite similar to that of ceramic sensors. The film is filled with micro-pores for water vapor condensation and some of the measurable physical properties change due to the water absorption [9].

Traditionally, according to sensing mechanisms, polymeric humidity sensors are divided into two fundamental categories: resistive-type and capacitive-type [11]. The resistive type reacts to different humidity levels by changing its conductivity while the capacitive-type changes its dielectric constant. Because polymer is highly sensitive to high temperature, almost all of the polymer-based humidity sensors are operated at room temperature. For resistive-type humidity sensors, one must modify the hydrophilic polymer to be insoluble in water while still maintaining the hydrophilicity to adsorb sufficient water molecules to form an ionic conduction path. Cross-linking

or graft-polymerization is a promising solution to this problem. The chemical procedure should be as simple as possible. On the other hand, in the case of a capacitive-type humidity sensor, the material used to fabricate sensor is hydrophobic polymers. It was found that the polymer should have as few micro-voids as possible so that the adsorbed water molecules are isolated in order not to form clusters that would cause hysteresis. In some cases cross-linking of the polymer chains was found to depress the clustering of water. In addition, the cross-linked polymers are durable in the presence of organic vapors. Humidity sensors based on conjugated polymers that are conductive polymers but not polymeric electrolytes attract considerable attention in research laboratories and industries [12, 13].

Resistive polymer-based sensors have a slower response though they are fast enough for most applications. The capacitive type has a broader operating temperature range than resistive types. Capacitive type can give good results down to 2% RH but sometimes less ideal than resistive type at RH level above 95%. Most capacitive types are more expensive but tend to be slightly more expensive than resistive types. The use of a resistive type or capacitive type is decided by application.

3.1.2 Ceramic Sensing Materials

Humidity sensors based on water-phase protonic ceramic materials are used widely in industry and research laboratories. The adsorbed water condensed on the surface of the materials and protons will be conducted in the formed aquatic layers. For ionic sensing materials, if the humidity increases, the conductivity decreases and the

dielectric constant increases [14, 15]. In bulk water, proton is the dominant carrier responsible for the electrical conductivity. The conduction is due to the Grotthuss mechanism, through which protons tunnel from one water molecule to the next via hydrogen bonding that universally exists in liquid-phase water.

There are four basic types of oxide-based sensing materials, including Al_2O_3 , TiO_2 , SiO_2 , and spinel compounds. Al_2O_3 is one of the most popular ceramic sensing material due to its relatively independence of temperature at all range of humidity from 25 °C to 80 °C [16]. There are several phases for Al_2O_3 but only two of them are used in humidity sensing: $\gamma\text{-Al}_2\text{O}_3$ (amorphous) and $\alpha\text{-Al}_2\text{O}_3$ (corundum). The former is more sensitive than the latter due to its high porosity. But $\alpha\text{-Al}_2\text{O}_3$ is more thermodynamically stable phase [9]. Al_2O_3 is also an important material for absolute humidity measuring, this will be talked later in this chapter. TiO_2 has three phases: brookite, anatase, and rutile. The first phase is rarely used in humidity sensing. If heated strongly (~1000 °C), anatase will automatically transforms to the rutile structure [17]. Actually Rutile is the most common phase of TiO_2 , anatase is very rare in nature. SiO_2 is not quite suitable for humidity sensing compared to other ceramic materials because it is a dense material. Humidity sensors based on porous silicon oxide were fabricated using bulk-sintering processes, especially traditional sol-gel method, in which SiO_2 is precipitated by hydrolysis of certain alkoxide of silane [18-20]. Similar to other porous ceramic materials, the humidity sensitivity of SiO_2 can be enhanced by adding electrolyte dopants, e.g. LiCl [21]. The spinel compounds

belong to a large group of oxides with a general composite of AB_2O_4 .

3.1.3 Semiconducting Sensing Materials

Some ceramic oxides or composite oxides such as SnO_2 , ZnO , and In_2O_3 , etc. are wide-bandgap semiconductors. H_2O is adsorbed on the oxide surface in molecular and hydroxyl forms. Water molecules are observed to increase the conductivity of n-type ceramics and to decrease the conductivity of p-type ceramics [22, 23]. This effect has been attributed to the donation of electrons from the chemically adsorbed water molecules to the ceramic surface [22]. Another mechanism was proposed [24, 25]. It was suggested that water molecules replace the previously adsorbed and ionized oxygen and therefore release the electrons from the ionized oxygen [24, 25]. Probably the “donor effect” could be resulted from both.

Because the conductivity is caused by the surface concentration of electrons, this sensing style is usually called “electronic type.” However, the water layer formed by the physical adsorption may be somewhat protonconductive. Therefore, at room temperatures the conductivity of ceramic semiconducting materials is actually due to addition of both electrons and protons (ionic), unless at high temperatures ($>100\text{ C}$) moisture cannot effectively condense on the surface. In Figure 3.1a, the conductivity increment is produced by surface electron accumulation resulting from the preferential alignment of the water dipoles [22]. Hydrogen atoms contact the surface (mostly at the oxygen sites) and attract electrons outward. In Figure 3.1b, a depletion region forms originally due to adsorbed oxygen and the released electrons may

neutralize the depletion. Since adsorbed water molecules increase the conductivity of n-type ceramic semiconductors, nearly all the published works deal with n-type ceramics.

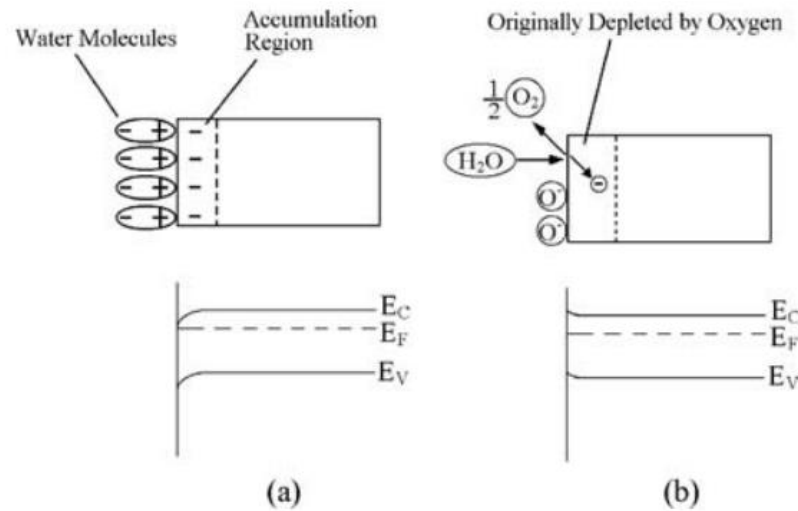


Figure 3.1 Two Possible Mechanisms For The “donor effect”

3.2 Absolute Humidity Sensors (Hygrometers)

3.2.1 Chilled Mirror Hygrometer

The chilled mirror hygrometer sometimes referred to as optical condensation hygrometer is the most accurate, reliable and fundamental device available to measure dew point. Dew point is detected by cooling a reflective condensation surface (a mirror) until water begin to condense, the temperature measured at this very moment is the dew point temperature, and the condensation phenomenon is detected by electro-optic detection system.

The surface temperature of a small gold mirror is controlled by a Peltier element (head pump), A high intensity light-emitting diode (LED) or sometimes laser light illuminates the mirror. The quality of reflected light from the mirror surface is

detected by a photo-transistor or optical detector. Another pair of LED and photo-transistor is used to compensate for the temperature deviation caused by the optical components. Photo-transistors are arranged in an electrical bridge circuit with adjustable balance which controls the current to the thermoelectric mirror cooler and, therefore, the mirror temperature. The Operation of the basic chilled mirror hygrometer is shown in the following figure.

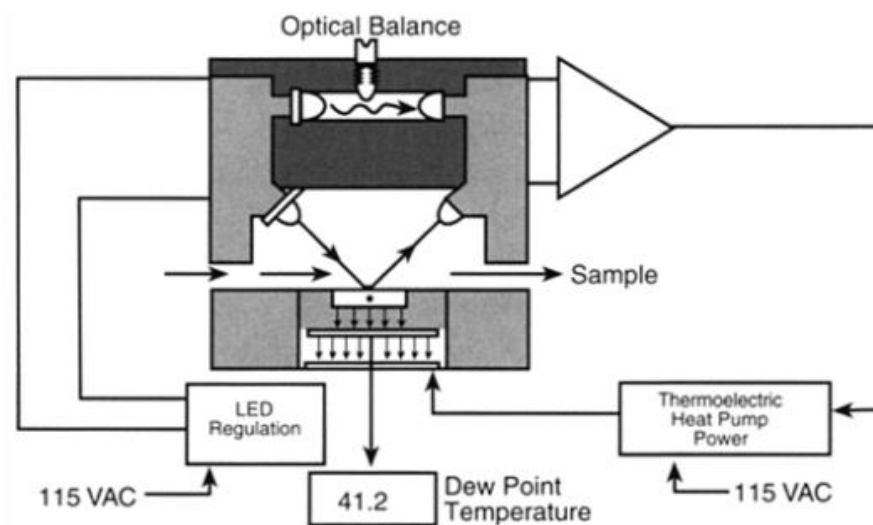


Figure 3.2 Schematic of Chilled Mirror Sensor

When the mirror surface temperature is above the dew point, no dew is formed on the mirror surface, so the reflectance is high and maximum light is received by the photo-detector. When the thermoelectric cooler lowers the mirror surface temperature below the dew or frost point, condensation would happen on the surface, which cause the light scattering, thereby reduce the amount of light received by the optical-receiver. The system is designed such that the bridge is balanced only when a pre-determined layer of dew or frost is maintained on the mirror surface. Under these equilibrium conditions, the surface temperature is precisely at the dew point of the gas passing

over the mirror. A precision NIST-traceable platinum or equivalent thermometer is embedded within the mirror surface to measure its temperature. When the mirror surface is clean, a perfect layer of condensation would occur right at the dew point such that we can get accurate and repeatable results. The temperature fluctuations around the dew point usually were not over 0.03 K [9].

Because of chilled mirror hygrometer's fundamental way of measuring dew point and it's the most accurate and reliable method available, it is widely used as a calibration standard. Despite all of these benefits, optical dew point hygrometers have several drawbacks, it is much more expensive than any other types of humidity measuring devices and requires maintenance by skilled personnel in monitoring and installation (such as providing proper sample flow). For this thesis research, I used another dew point transmitter to calibrate, FA410 (CS Instrument –Shenzhen, China), which is a polymer humidity sensor. This sensor is not sensitive at low humidity levels so actually it's not suitable as a standard to calibrate other sensors. But for the time being, I use it for research purposes and the accuracy provided is within tolerance. Ultimately, more fundamental and accurate calibration standard should be used, like using chilled mirror hygrometer instead.

3.2.2 Alpha-Alumina Humidity Sensor

In the previous sections, I've talked about relative humidity sensors, many of them suffered from serious drawbacks, e.g. long term instability, large humidity hysteresis and slow response, few of them are found to be effective for practical application.

Only aluminum oxide thin film sensor can be used for absolute humidity [26-29], which is especially useful in the trace moisture measurement range. By anodization of aluminum in H_2SO_4 solution, the porous alumina film with very high humidity-sensitivity is formed. Aluminum oxide sensors offer many advantages: wide dynamic range of humidity measurement, relatively stable with low hysteresis and temperature coefficients, low or modest maintenance requirements, available in small sizes, and it is capable of measuring very low dew point levels without the need for cooling like chilled mirror hygrometer needs.

Unfortunately, alumina humidity sensors have a serious flaw, that is, long-term calibration drift [30]. Many researchers try to solve this problem by aging the alumina films in boiling water or macerating the film in some ion solutions [30], however the drift can not be completely eliminated. The humidity-sensing film in the alumina sensors that suffered from this type of drawback is made of $\gamma\text{-Al}_2\text{O}_3$ (amorphous). $\gamma\text{-Al}_2\text{O}_3$ changes to $\gamma\text{-Al}_2\text{O}_3 \cdot \text{H}_2\text{O}$ (Boehmite) irreversibly under high humidity atmosphere [9]. Which causes the surface area and porosity of the film to decrease. This further gradually decreases the adsorption ability of the film and causes the long-term calibration drift.

Previous research has been made by my advisor Dr. Zhi Chen to use $\alpha\text{-Al}_2\text{O}_3$ thin films [9]. It was found that humidity sensors made of $\alpha\text{-Al}_2\text{O}_3$ films have the potential to solve this problem. Usually, we can get $\alpha\text{-Al}_2\text{O}_3$ by heating $\gamma\text{-Al}_2\text{O}_3$ at a temperature over $1200\text{ }^\circ\text{C}$, in his research, $\alpha\text{-Al}_2\text{O}_3$ was obtained by anodization of

aluminum plates in the melt of $\text{NaHSO}_4\text{-KHSO}_4$ (1:1 wt.) at 200 °C. I will not go over the details of fabrication, however I'll show the performance characteristics of the sensors. The schematic structure of the sensor is shown in figure 3.3. The $\alpha\text{-Al}_2\text{O}_3$ films were reanodized to form a thin barrier film (amorphous Al_2O_3) at the pore base. A thin water-permeable gold film was deposited by vacuum evaporation on one of the surfaces of the sample, which was used as one electrode, the other electrode was the aluminum substrate.

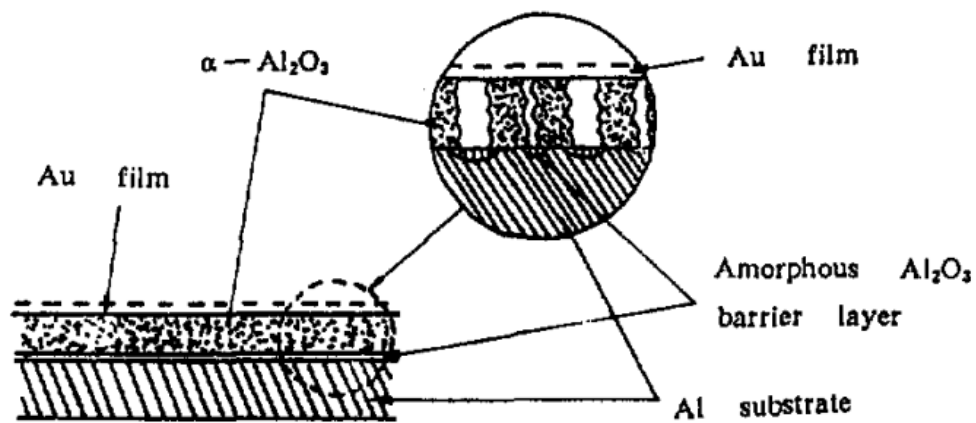


Figure 3.3 Schematic Structure of Alpha-Alumina Humidity Sensor

The following figure show the porous $\alpha\text{-Al}_2\text{O}_3$ film prepared by anodic spark deposition, the film exhibits a continuous open pore structures as mentioned earlier. Unlike $\gamma\text{-Al}_2\text{O}_3$, $\alpha\text{-Al}_2\text{O}_3$ is highly stable, so the inner surface of the pores and pore size never changes over time, make it ideal for humidity measurement [9]. The possible instability may come from the amorphous alumina barrier layer.

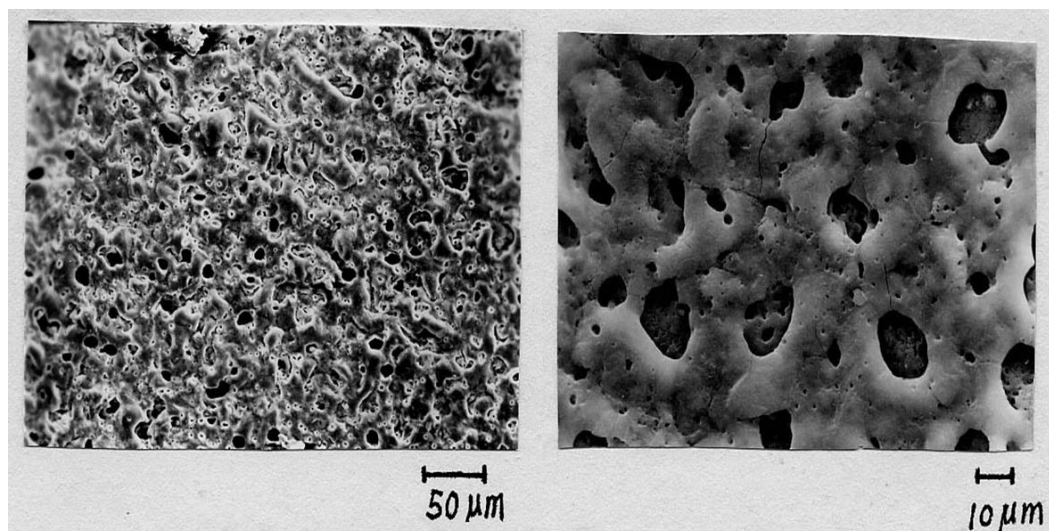


Figure 3.4 Scanning Electron Micrographs of an
Anodic Spark Deposited α -Al₂O₃ Porous Film

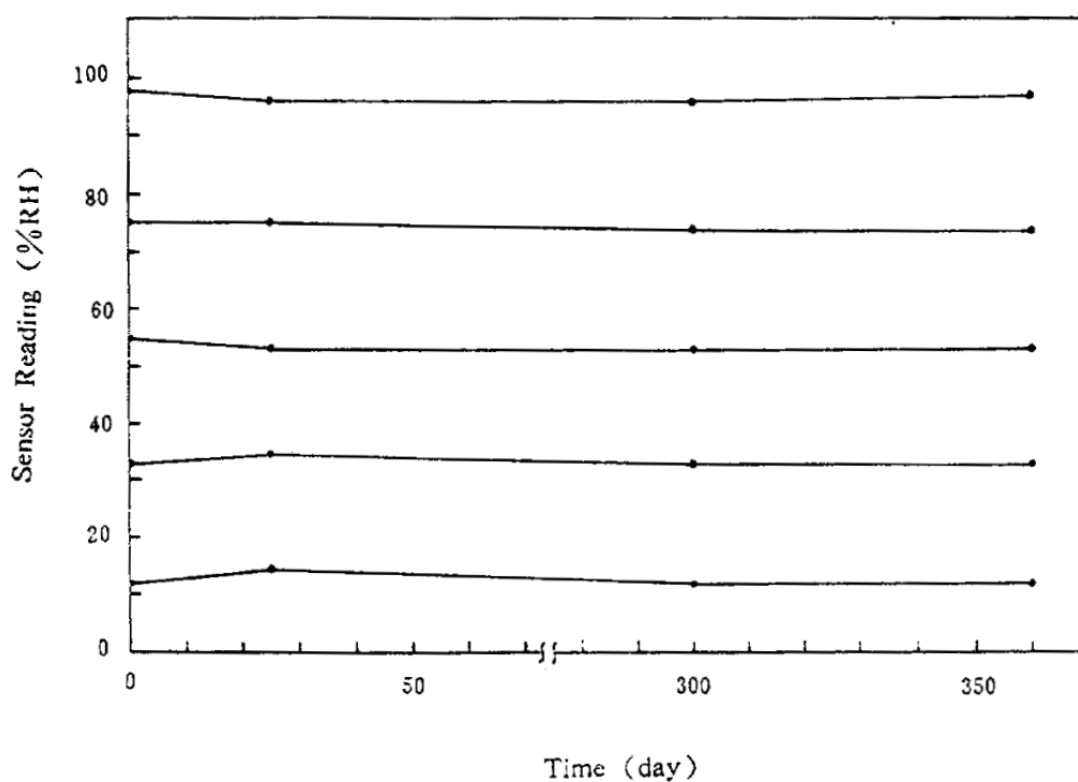


Figure 3.5 Long Term Stability Testing Result of RH Measurement

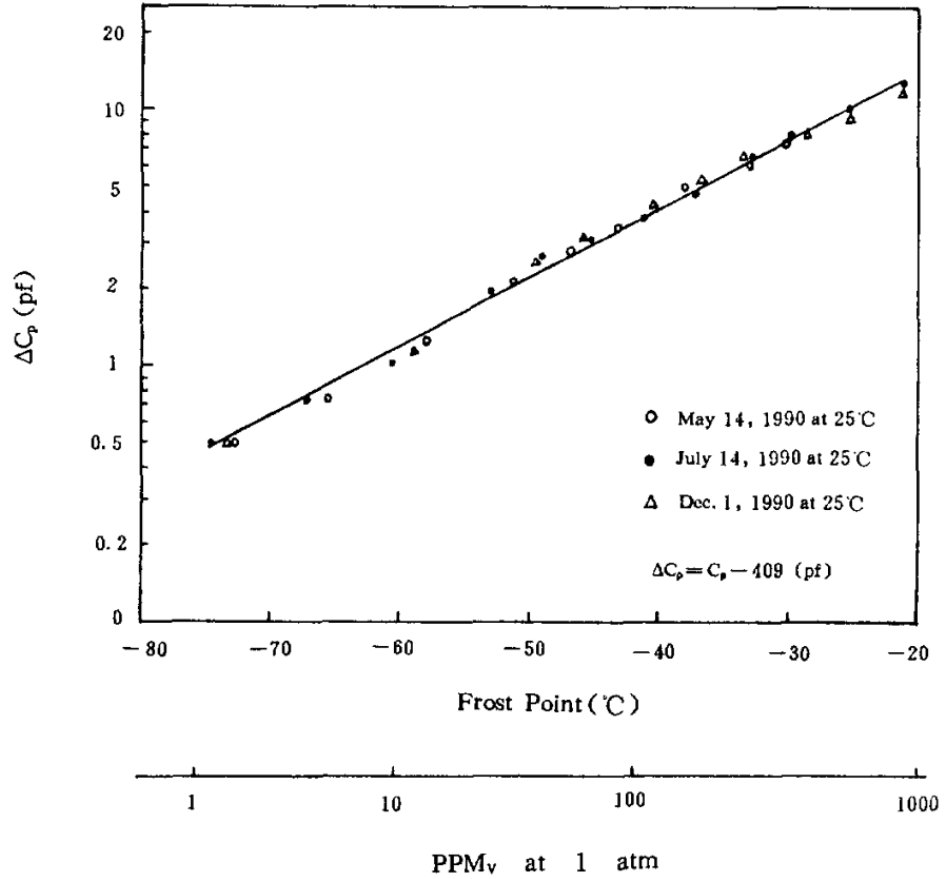


Figure 3.6 Long Term Stability Testing Result of Absolute Humidity Measurement

The previous two pictures show the long-term stability of the sensor made from $\alpha\text{-Al}_2\text{O}_3$ thin film both in relative humidity measurement and absolute humidity measurement. In the relative humidity experiment, after long time exposure in 97%RH environment and reset it in low humidity environment, the sensor can still give the previous readout [9]. This fact indicate that there was no hydroxide formed on it (chemisorption), the water vapor was only physically adsorbed on the porous surface of the modified $\alpha\text{-Al}_2\text{O}_3$ thin film.

The response of this type of sensor is also very quick, the following figure shows that for a 63% RH change, the response time is about 5 seconds. This may be attributed to the lack of chemisorption on the surface of the film.

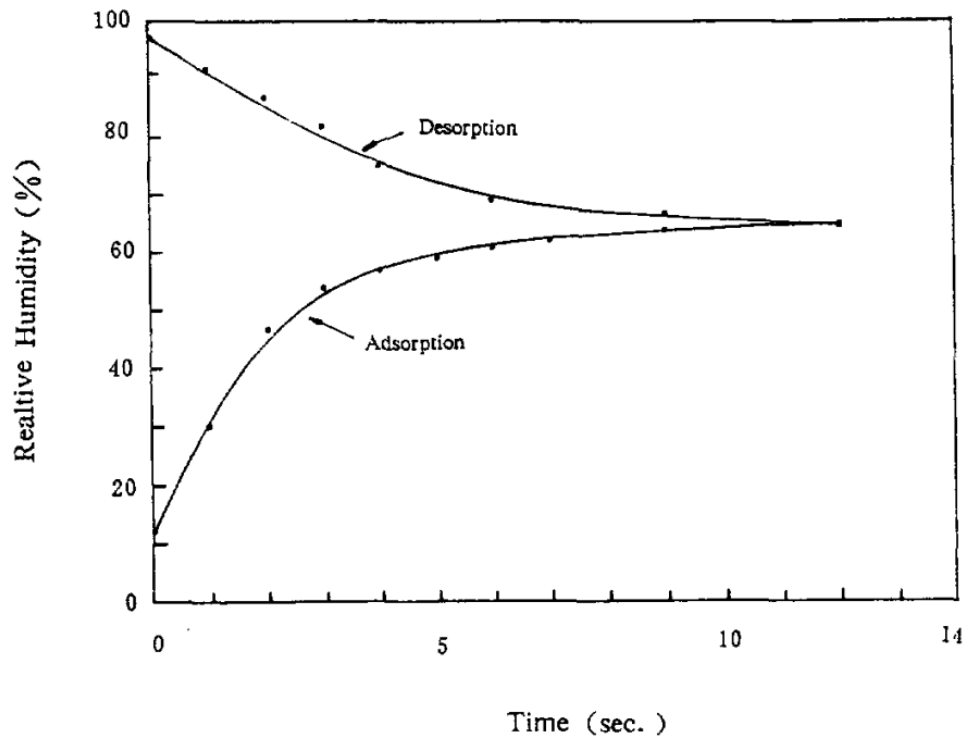


Figure 3.7 Time Response Characteristics of RH variations

The temperature dependency of alumina sensors are modest compared to other materials, however this $\alpha\text{-Al}_2\text{O}_3$ humidity sensor do show temperature dependency. It is shown in the following figure, we notice that the temperature coefficient of the sensor varies with temperatures, it has a higher temperature coefficient at higher temperatures, one of the purposes of this thesis research is to find a way to compensate this temperature coefficient thus the sensor can give right readouts under different temperature environment.

Figures 3.3-3.8 are from Dr. Zhi Chen's previous research results at University of Electronic Science & Technology of China [9]. Recently, at University of Kentucky and Advanced Semiconductor Processing Technology, LLC, Dr. Zhi Chen further investigated the alpha-alumina moisture sensors and found that they still exhibited some calibration drift, which is due to the amorphous alumina barrier layer. He

further improved the alpha-alumina moisture sensors by eliminating the amorphous alumina barrier layer. The new sensors exhibited superior performance with fast response of ~3s, little hysteresis, and true long-term stability (US and Chinese patents pending). I will use the new sensors for calibration studies.

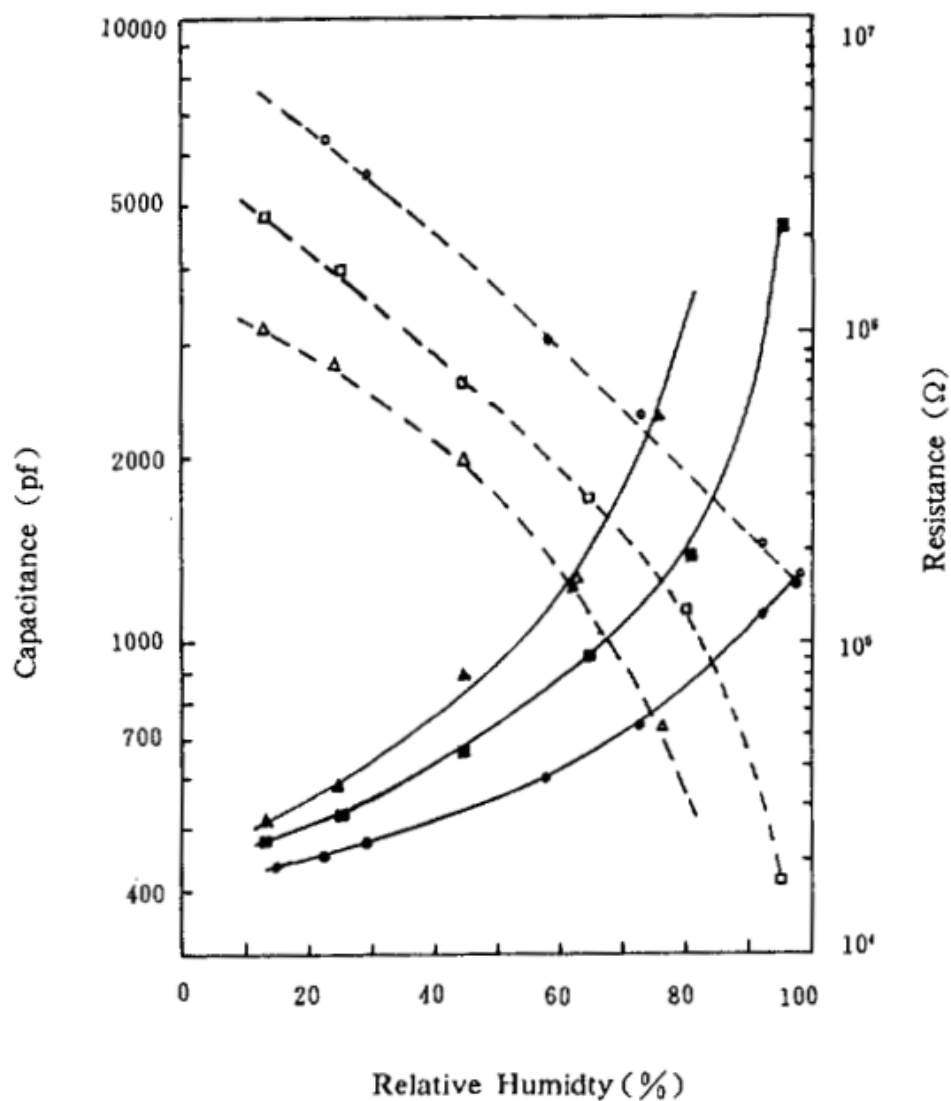


Figure 3.8 Temperature Dependence of the Sensor

Chapter 4 Dedicated Embedded System

In this chapter, the original dedicated embedded system for this sensor is introduced. It was developed with a msp430 microcontroller manufactured by Texas Instrument Inc. which incorporates a 16-bit RISC architecture CPU and many digital and analog peripheral modules to facilitate mixed signal processing applications, and it provides several low power operation modes enables it a good choice for battery powered portable devices. The calibrated digitally controlled oscillator (DCO) allows wake-up from low-power modes to active mode in less than 1 μ s. The modules of the circuits and peripherals utilized in the microcontroller will be discussed in detail.

4.1 Msp430 Architecture and Peripherals

Figure 4.1 shows the architecture of the MSP430F249, on the left is the CPU and its supporting hardware, including basic clock generator, emulation and JTAG interface

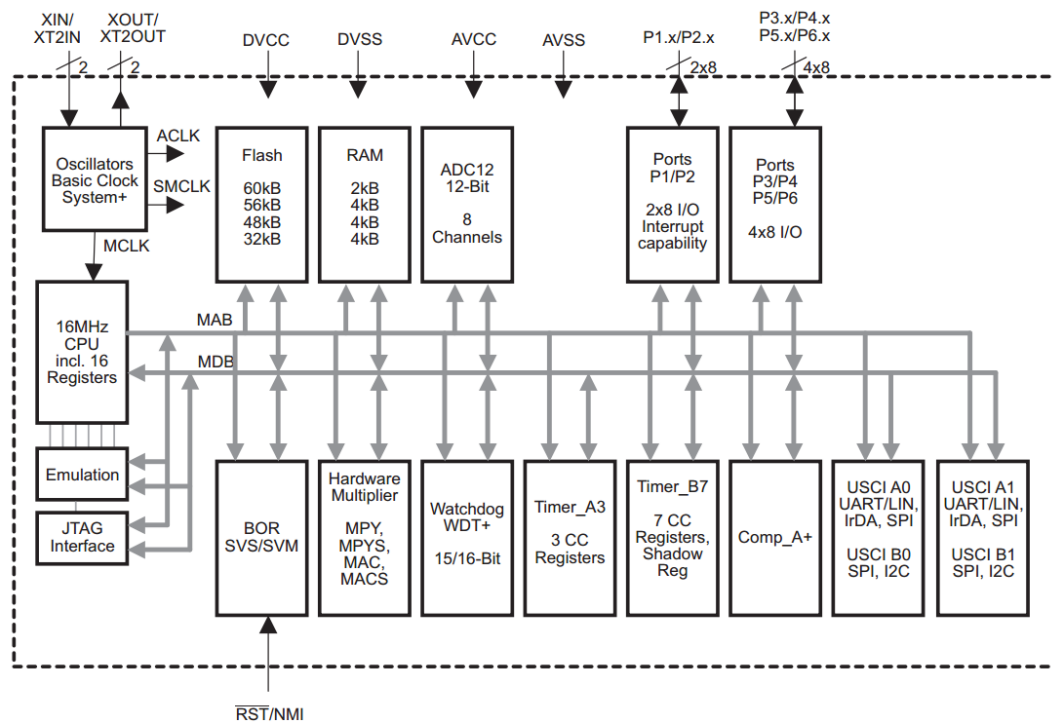


Figure 4.1 Block Diagram of the MSP430F249 taken from datasheet

which is used to communicate with a computer for program downloading or debugging. Other main blocks are linked by two buses, one is the memory address bus (MAB), and the other is memory data bus (MDB). For MSP430F29 the microcontroller this project is using, it has 60KB+256B flash memory and a 2KB ram, that's enough storage space for project code. The ADC12 peripheral, Timer_A3 peripheral, and Comparator_A+ peripheral make it capable of dealing with outside analog signals, the single slope A/D conversion used here is one example of using Timer_A3 and Comparator_A+ together. The microcontroller also incorporates many other useful peripherals like watchdog timer, hardware multiplier, SPI, I2C, UART, etc.

4.1.1 Basic Clock Module

All microcontrollers have a basic clock module to drive the CPU and peripherals, it is an essential part for every synchronous digital system. Two clocks with different specifications are often needed: one fast clock to drive CPU, which can be started and stopped rapidly to conserve energy, usually it need to be very accurate; another slow clock that runs continuously to monitor real time, which must consumes little energy and be particularly accurate. The MSP430 meet the conflicting demands for high performance, low power, and a precise frequency by using three internal clocks, which can be derived from up to four sources are available for the clock as shown in figure 4.2 (source: msp430x2xx datasheet).

LFXT1: Low/high frequency crystal oscillator, it can be used with a low frequency

watch crystal (32 KHz), also can run with a high frequency crystal (up to 16 MHz).

XT2: High-frequency crystal oscillator, it is similar to LFXT1 but restricted to high frequencies.

VLO: Internal very low-power, low-frequency oscillator, it provides an alternative to LFXT1 when the accuracy of a crystal is not needed.

DCO: Digitally controlled oscillator, it is a controllable RC oscillator that starts in less than 1 μ s.

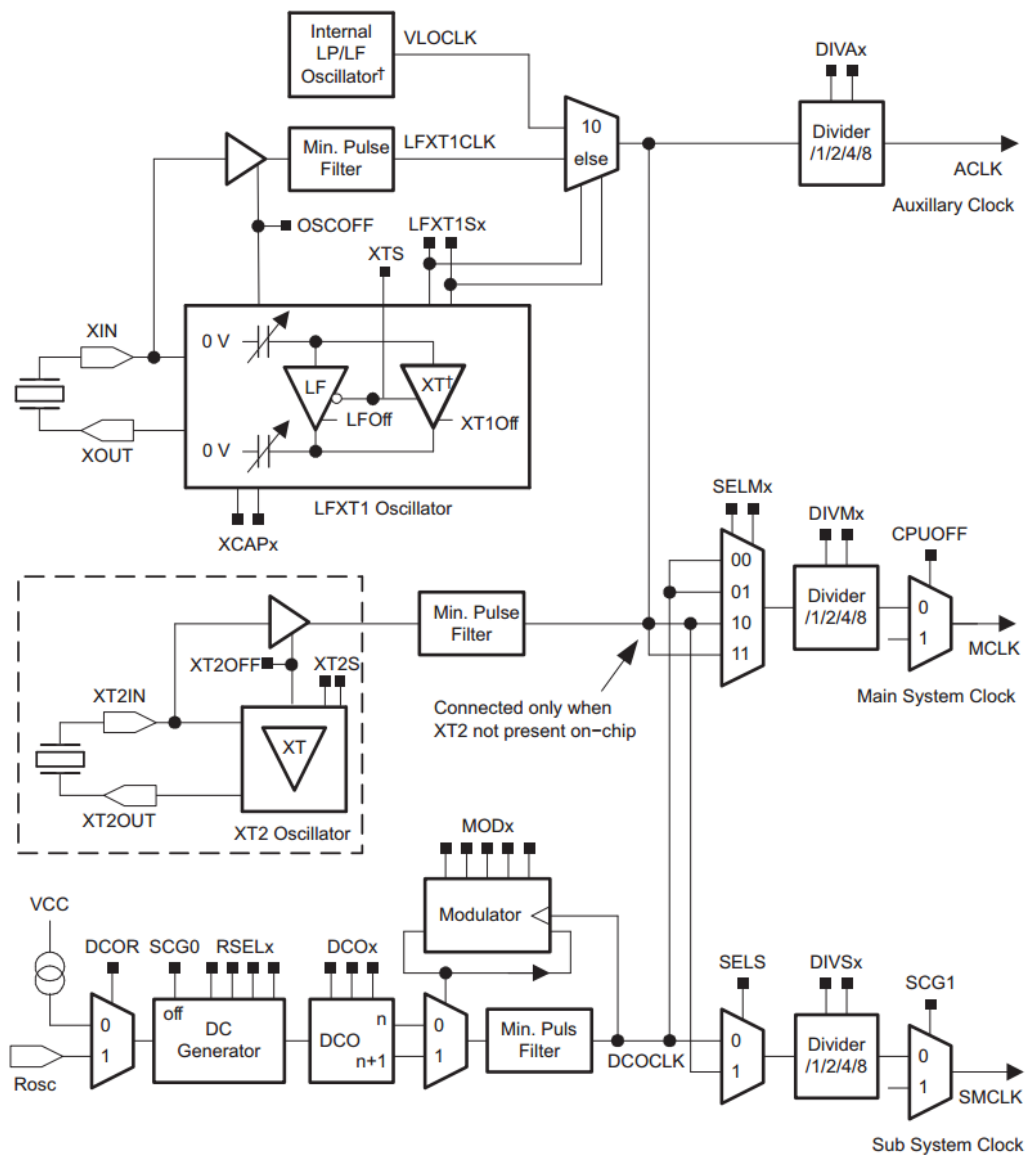


Figure 4.2 Basic Clock Module Block Diagram for MSP430F249

Below are three internal clocks

MCLK: Master clock, it is used by CPU and a few peripherals.

SMCLK: Subsystem master clock, it is distributed to peripherals.

ACLK: Auxiliary clock, it is also distributed to peripherals.

Figure 4.3 shows a simplified block diagram of the clock module of MSP430F249

[31], three internal clocks all can be divided by 1, 2, 4 or 8. Their selecting sources

are shown on this figure, Heavy lines indicate the default configuration.

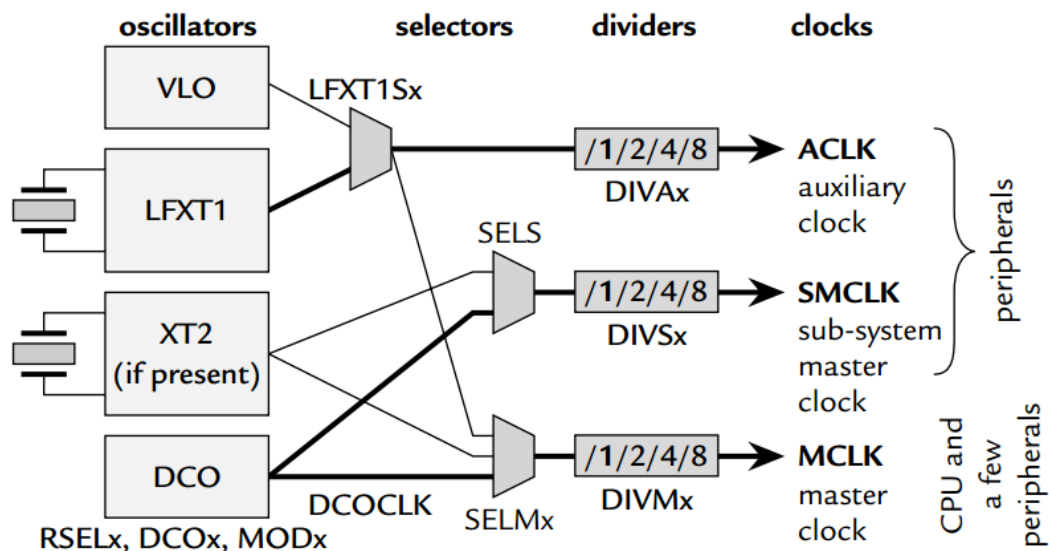


Figure 4.3 Simplified Block Diagram of the Clock Module

The basic clock module is controlled by four registers, DCOCTL and BCSCTL1-3. In

addition there are bits in special function registers IFG1 and IE2 for reporting faults

with the oscillators.

4.1.2 Timer_A3

Timer_A is the most versatile, general-purpose timer in all MSP430 microcontrollers,

it is a 16-bit timer/counter with three capture/compare registers. It has many useful

features and plays an important role in single slope A/D conversion which will be

introduced later this chapter. There are two main parts in this peripheral.

One is the timer block, based on a 16-bit register TAR. It can choose from different clock sources: TACLK, ACLK, SMCLK, and INCLK whose frequency can then be divided down. The timer block has no output but a flag TAIFG used to trigger an interrupt. It has four modes of operation, selected by MCx bits, the 16-bit timer/counter register TAR increments or decrements with each rising edge of the clock signal depending on mode of operation: When under stop mode, the timer is halted; under continuous mode, the counter runs its full range from 0x0000 to 0xFFFF and then run back to 0; under up mode, the counter runs from 0 up to the value stored in TACCR0; under up/down mode, the counter counts from 0 to TACCR0 then down to 0 and repeats. Figure 4.4 shows the basic timer block of Timer_A from MSP430x2xx datasheet.

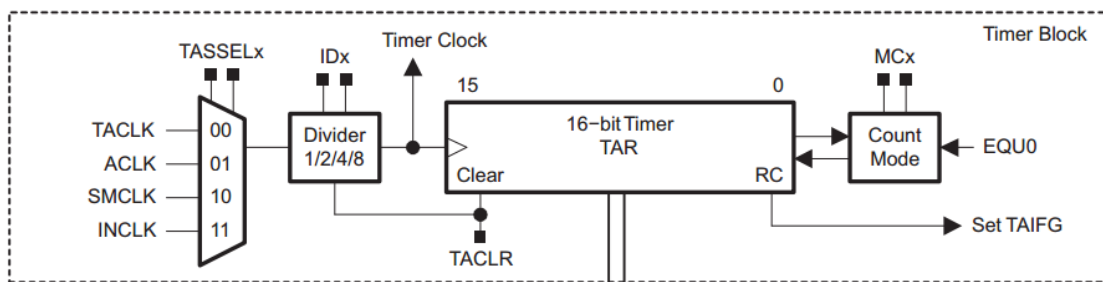


Figure 4.4 Basic Timer Block of Timer_A3

The other part is capture/compare channels, for MSP430F249 three channels are available. All channels within Timer_A share the same timer block, that is, there is only one TAR. This ensures that all actions performed by the different channels are synchronized. But the downside is they all work at the same frequency. Capture and compare channel 0 is special in two ways. First its register TACCR0 is used for the

modulus value in Up and Up/down modes. Second it has its own interrupt vector with a higher priority than the other interrupts from Timer_A, which all share a common vector TAIV. So channel 0 is often used with the most urgent tasks if it is free. Other channels work in the same way, they can perform the following tasks [31]:

1. Capture an input, which means recording the “time” (value in TAR) when the input changes at TACCRn, the input can be external or another internal peripheral or software. We’ll see later that the Comparator_A+ gives this input in the single slope A/D conversion.
2. Compare the current TAR value with the value stored in TACCRn and give an output when they match.
3. Request an interrupt by setting its flag TACCRn CCIFG.

Figure 4.5 shows the block diagram of capture/compare channel 2:

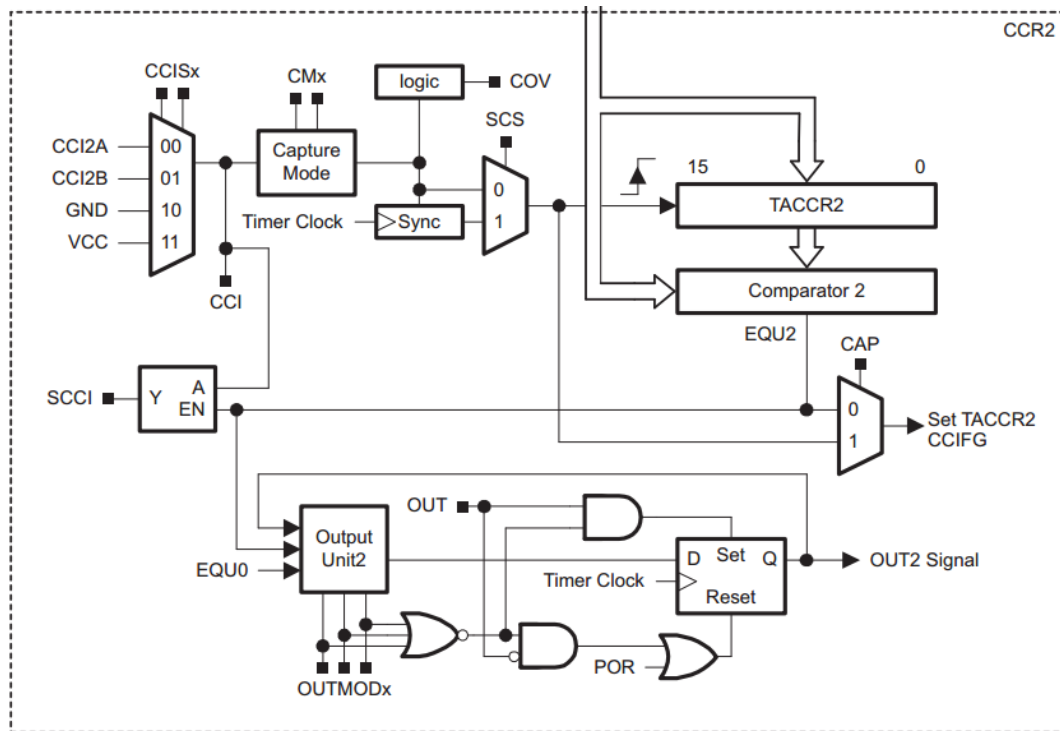


Figure 4.5 Block Diagram of Capture/Compare Channel 2

Each channel is controlled by a register TACCTLn, shown in the following figure.

15	14	13	12	11	10	9	8
CMx		CCISx		SCS	SCCI		CAP
7	6	5	4	3	2	1	0
OUTMODx			CCIE	CCI	OUT	COV	CCIFG

Figure 4.6 Timer_A Capture/Compare Control Register TACCTLn

The CAP bit is cleared by default so that the channel is in compare mode, because the capture mode is being used in the research, we need to set it to 1. The capture mode bits CMx can choose an event to be a rising edge, falling edge, or either edge. The CCISx bits in TACCTLn select the input to be captured, CCInA and CCInB come from outside the timer module. Often CCInA is connected to external sources while CCInB is connected internally to another module. They have many possible connections, for MSP430F249 CCI1B come from CAOUT, the output of the comparator. This internal connection between peripherals allows precise time recording of a measurement without the delay that would rise if software were needed to trigger a capture when CAOUT changed. This is one example of the SoC idea of the MSP430 which makes peripherals to work together effectively. It saves power while avoiding delay.

Same as other peripherals, interrupts are an important part of Timer_A. interrupts can be generated by timer block itself (flag TAIFG) or by each capture/compare channel (each TACCRn CCIFG). TACCR0 has its own interrupt vector TIMERA0_VECTOR, it priority is higher than the other vector TIMERA1_VECTOR, which is shared by the remaining capture/compare channels and the timer block. The CCIFG0 flag in

TACCR0 is cleared automatically when its interrupt is serviced but this does not happen for the other interrupts because the interrupt service routine (ISR) need to determine the source of the interrupt. The MSP430 provides an interrupt vector register TAIIV to identify the source of the interrupt rapidly. When one or more of the shared interrupts flags is set, TAIIV is loaded with the value corresponding to the source with the highest priority. The following table shows the possible values in TAIIV for Timer_A3 [31]:

Table 4.1 Interrupt Vector Register TAIIV for Timer_A3

TAIIV contents	Source	Flag	Priority
0x0000	No interrupt pending		
0x0002	Capture/compare channel 1	CCIFG1	Highest
0x0004	Capture/compare channel 2	CCIFG2	
0x0006	—		↑
0x0008	—		
0x000A	Timer overflow	TAIFG	Lowest

Any access to TAIIV would resets TAIIV and the corresponding flag. If another interrupt is pending, TAIIV is reloaded with the value for the source with the highest priority and another interrupt is requested as soon as the current one is serviced.

4.1.3 Comparator_A+

An analog comparator compares the voltage on its two input terminals, V_+ and V_- . Its output is high if $V_+ > V_-$ and low if $V_+ < V_-$. Because the output has only two

states, this makes it act like a 1-bit ADC. The Comparator_A+ module is switched on and off with the CAON bit. It is off by default to save power. Although a comparator is fairly simple, the block diagram in the datasheet looks a little complicated:

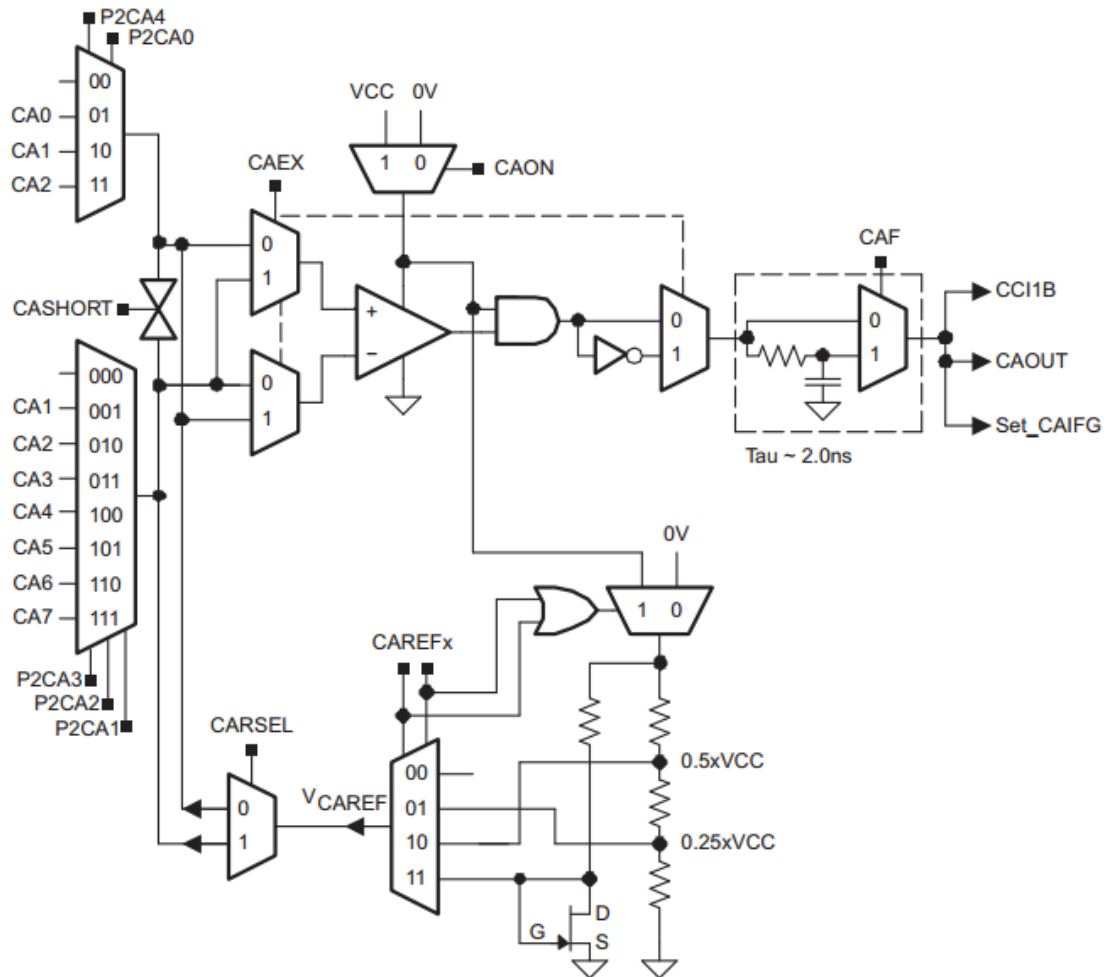


Figure 4.7 Comparator_A+ Block Diagram

The non-inverting terminal V_+ can be connected to external signals CA0-CA2 or left unconnected, this is selected using bits P2CA4 and P2CA0. It can also receive an input from internal reference.

Similarly, the inverting terminal V_- can be connected to external signals CA1-CA7 (not include CA0) or left unconnected. This is selected by bits P2CA3-P2CA1. It can also be connected to an internal reference.

The internal reference voltage V_{CAREF} can be chosen from $1/4 V_{\text{CC}}$, $1/2 V_{\text{CC}}$ or a nominally fixed voltage from a transistor, V_{diode} . This is selected with CAREFx bits. It can be applied to both of the comparator terminals, selected by CARSEL bit.

The output of comparator can be optionally filtered through an RC circuit to reduce oscillations in the signal. This is selected with CAF bit. It is off by default but should usually be enabled unless the delay it introduces is unacceptable or any oscillation is handled in software. The filter extends the response time from approximately $0.2\mu\text{s}$ to $2\mu\text{s}$. In this application, it is set off because it is time critical.

The output is brought to an external pin CAOUT. It is also connected internally to capture input CCI1B of Timer_A, which allow them to work together nicely without delay.

CAIE and GIE need to be set in order to request an interrupt. The flag CAIFG is raised on either a rising or falling edge of the comparator output selected with CAIES bit.

Because for a real comparator it is not perfect and has a small offset voltage, this means the output does not switch exactly at $V_+ = V_-$ but occur when they differ by a small voltage between $\pm 30\text{mV}$. Setting the CAEX bit exchanges the two inputs to the comparator and inverts its output to compensate

4.2 Single Slope A/D Conversion

As mentioned above, the single slope A/D conversion technique is implemented with Comparator_A+ and Timer_A3. There is a very good example shown on msp430x2xx

family user guide of using single slope analog-to-digital conversion to precisely measure resistive elements [32]. By comparing the measured resistor's capacitor discharge time to that of a reference resistor shown in the following figure, we can further calculate the R_{means} based on R_{ref} .

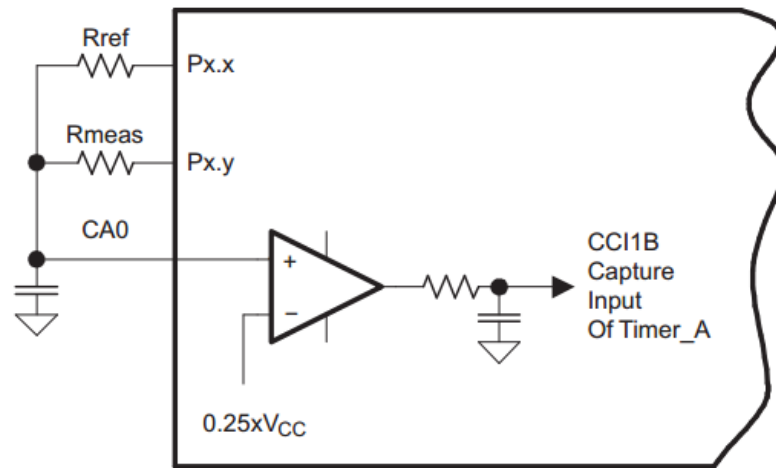


Figure 4.8 Resistance Measurement Schematic

Two I/O pins are connected to R_{ref} and R_{meas} respectively, set I/O pin to output high (V_{cc}) would charge the capacitor, reset to low would discharge the capacitor. The + terminal of the comparator is connected to the positive side of the capacitor and – terminal of the comparator connected to a reference voltage, for example, $0.25 \times V_{cc}$. $CAOUT$ is connected to Timer_A CCI1B, capturing capacitor discharge time. The following figure shows the timing of this process [32].

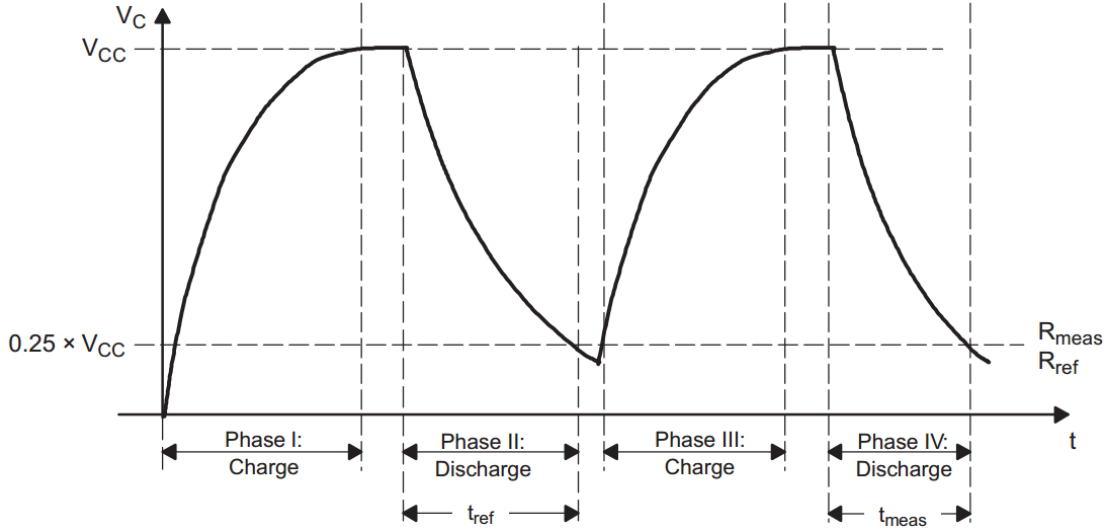


Figure 4.9 Timing of Resistance Measurement Systems

The equation below shows the voltage change of a discharging RC circuit:

$$V_C(t) = V_{CC} \exp(-t/RC)$$

If we make $V_C(t)$ to a reference voltage we can get discharge time to that voltage:

$$t = -R \times C \times \ln(V_{ref}/V_{CC})$$

After two discharging process of two resistors respectively we get two discharging times of two resistors respectively:

$$t_{meas} = -R_{meas} \times C \times \ln(V_{ref}/V_{CC})$$

$$t_{ref} = -R_{ref} \times C \times \ln(V_{ref}/V_{CC})$$

Remember the Timer_A is actually just a counter, let N be the number which Timer_A counts the discharging process, and apparently we have:

$$\frac{N_{meas}}{N_{ref}} = \frac{t_{meas}}{t_{ref}}$$

Based on the ratiometric conversion principle

$$\frac{N_{meas}}{N_{ref}} = \frac{-R_{meas} \times C \times \ln(V_{ref}/V_{CC})}{-R_{ref} \times C \times \ln(V_{ref}/V_{CC})}$$

We can finally get R_{meas}

$$R_{meas} = R_{ref} \times \frac{N_{meas}}{N_{ref}}$$

For measurement of capacitances, the exact same circuits and techniques are used except that the resistor here is a fixed one, and we also need a reference capacitor. For our application of measuring humidity sensor for dew point we don't need to get this actually capacitance, we can just relate the clock cycle's value with dew point. That is, N_{meas} is all we need. When surrounding humidity changes, the capacitance of humidity sensor changes, result in the change of value returned from TACCRx indicating different dew point levels. Further modeling is needed in order to relate the "circuit value" with dew points, this will be described in following chapters.

4.3 Temperature module

Because we want to test the humidity sensor's behavior under different temperatures, the temperature measurement module is obviously indispensable. It has to be small in size so that it can be placed next to a humidity sensor inside the filter. A variety of temperature sensors were considered, however few are suitable for this humidity transmitter. DS18B20 for example is a widely used temperature sensing component but its size is too big to fit into the air filter together with our humidity sensor. Another option like precision thermistor (NTC or PTC) has a small size that can be fit into air filter but the non-linear property with temperature makes it difficult to calibrate. So it is not ideal either.

A different but simple temperature sensing technique based on diodes is used here. The following figure shows the calculated diode characteristics using SPICE model

for temperatures $T = 100\text{ }^{\circ}\text{C}$, $T = 27\text{ }^{\circ}\text{C}$ AND $T = -50\text{ }^{\circ}\text{C}$ [33].

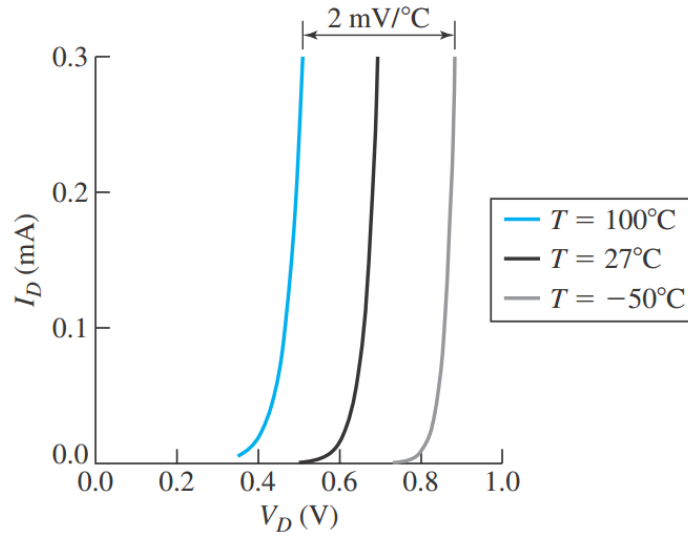


Figure 4.10 Temperature Dependence of the Diode Characteristics

We can see that the temperature basically shifts the I_D - V_D characteristic along the V_D axis by approximately $-2\text{mV}/^{\circ}\text{C}$. Because the coefficient is negative, to produce the same current an $1\text{ }^{\circ}\text{C}$ increase in temperature the forward voltage would drop about 2mV . This linear relation between forward voltage and temperature can be utilized to measure temperature, the remaining problem is how to detect forward voltage changes precisely. Many ADC converters can capture the analog voltage change and output digital data that can be processed by microcontroller. However the full range of voltage variation is small even temperature differs dramatically. So an op-amp is used to amplify the voltage change to make it easier to be identified. The following figure shows the implemented temperature module schematic.

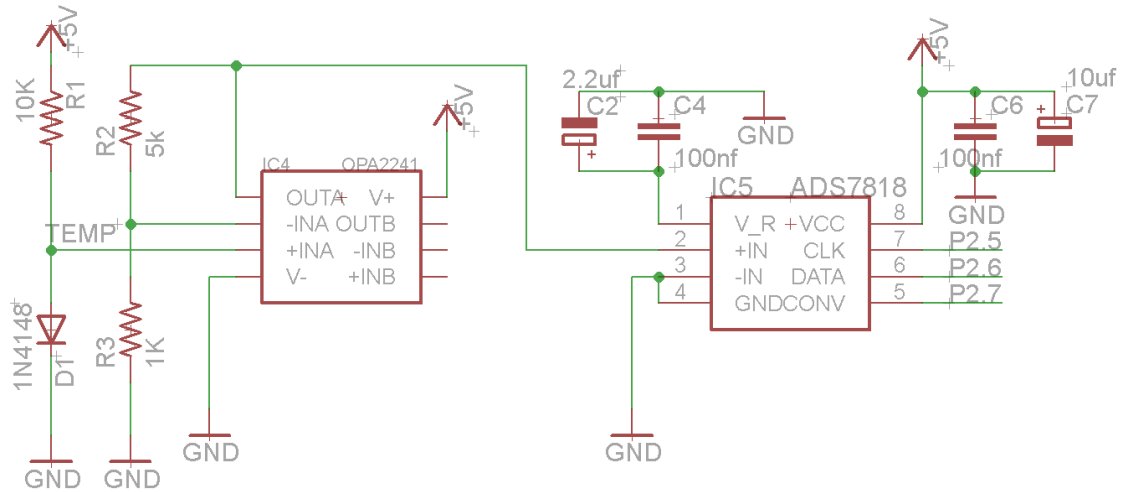


Figure 4.11 Schematic Diagram of Temperature Module

1N4148 is a fast speed diode featuring small size, fast switching speed and fast reverse recovery. The voltage across the diode is connected with the non-inverting of the op-amp. +5V voltage supply the R1 and diode. The closed-loop gain is $(1 + R2/R3) = 6$. So the temperature coefficient is amplified to 12mV/ °C on the output terminal of op-amp. The op-amp OPA2241 from Texas Instruments features wide supply range, high open loop gain, low offset voltage and low power consumption. The output of OPA2241 is still analog signal. An ADC ADS7818 is used here.

ADS7818 is a 12-bit high speed successive approximation (SAR) analog-to-digital converter. The range of the analog input is set by the voltage on V_{REF} pin. With internal 2.5V reference, the input range is 0 to 5V. The digital result of conversion is provided in a serial manner, synchronous to the CLK input. The result is provided most significant bit first.

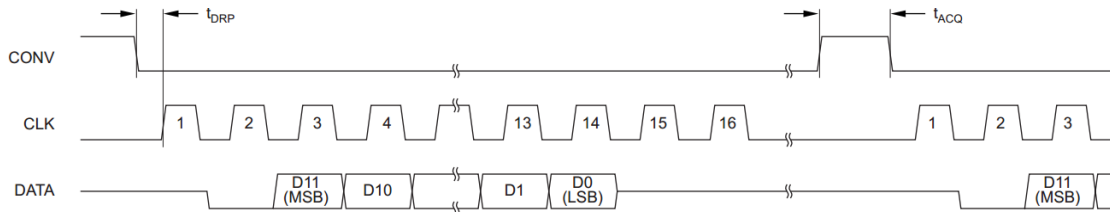


Figure 4.12 Typical SPI Timing Interface

Figure 4.11 shows a typical timing diagram for a serial peripheral interface (SPI).

CONV, CLK, DATA pins of ADS7818 are connected to I/O pins of MSP430F249.

The transition of high to low on CONV pin indicates the beginning of the transition.

After second clock cycle, the 12-bit are read into microcontroller. The biggest number a 12-bit can represent is 4095, so from 0 to 4095 the full voltage range is divided in to 4096 pieces. We have the following equation:

$$V_{meas} = O_c \times (FS/4096)$$

Where O_c is the output number of ADS7818, FS is full scale voltage range, $FS = 2 *$

$V_{REF} = 5V$. From this equation we can calculate the amplified voltage.

Then the temperature can then be calculated as follow:

$$T = \frac{|\left(\frac{V_{meas}}{n}\right) - V_{ref}|}{2mV}$$

Where n is the gain of OPA2241, in this case 6. V_{ref} is the voltage across the diode at a known temperature, for example we can test this value when diode is put into mixture of ice and water that is sure to be 0 °C.

Chapter 5 Sampling System Design

Calibration is perhaps the most significant procedure in the production process of a good aluminum oxide humidity sensor. In order to calibrate our alpha alumina humidity sensor we need to design a sampling system, so that we can test it and compensate the temperature coefficient. Some big humidity sensor manufacturers have built very elaborate calibration systems that can calibrate multiple sensors simultaneously. The data of the sensors are stored in computer, and the calibration process is repeated several times within 3 to 6 months. Not until the calibration data showed reasonably stable, such sensor cannot be installed. Figure below shows a typical commercial aluminum oxide calibration facility [1].

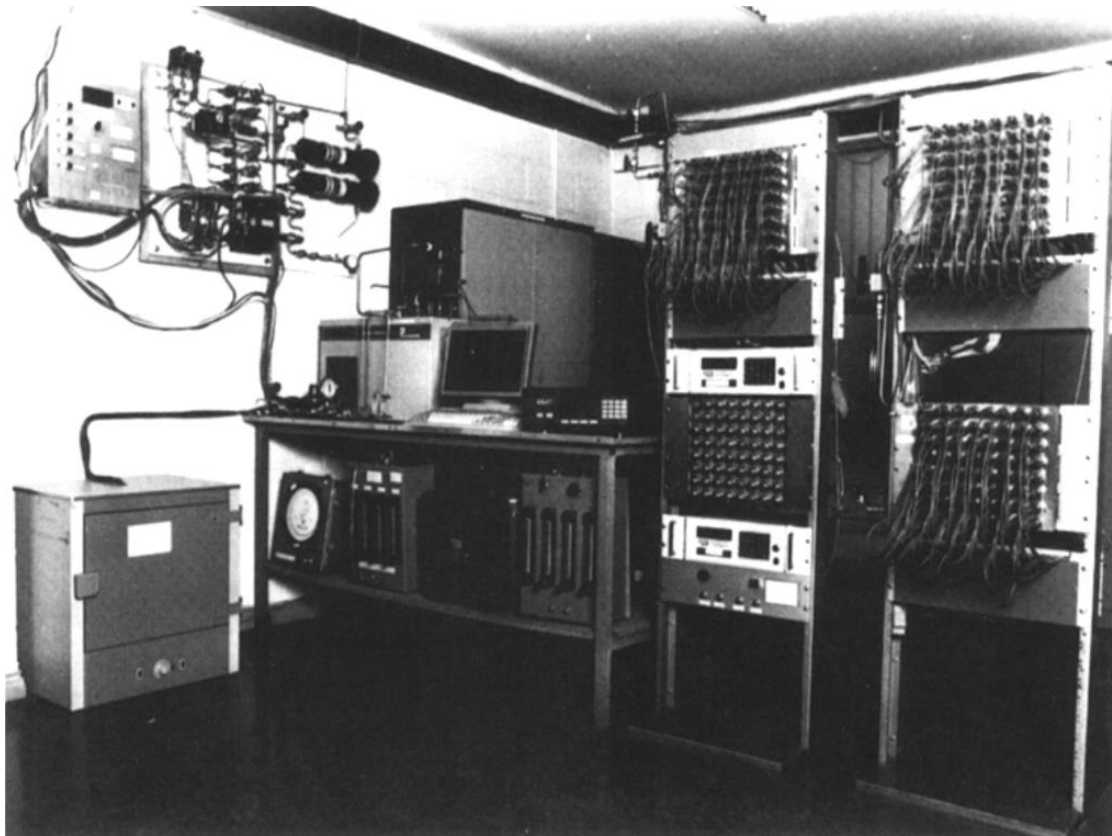


Figure 5.1 A Calibration Laboratory of Aluminum Oxide Sensor

Although such calibration system is very capable and efficient in calibrating aluminum oxide sensors, they are too complicated and high in expense. In present laboratory conditions, we have to implement an economic calibration system that is dedicated for our alpha-alumina humidity sensor. The sample tested gas is provided by ultra-high purity nitrogen gas, such gas is guaranteed to be blow 3 PPM of humidity level. So the tested nitrogen gas has a dew point of below -69 °C, dry enough for our experiment purposes.

5.1 Peltier Effect

In order to test the sensor under different temperatures, one of the requirement arises is that we need a facility that can adjust its temperature. The first idea was to change a mini refrigerator to let it have the ability of warming up, or change an oven to let it have the cooling ability. But this is difficult to do than it may sound. It would be great if I can find a device that can vary temperature from 0 °C and 50 °C. It caught my attention that the Peltier device used in a mirror-based hygrometer can nicely adjust and control the temperature. The thermoelectric effect behind the Peltier device may offer an alternative approach in temperature control applications.

When a semiconductor is used as a thermoelectric material, its majority charge carriers (electrons or holes) determine the electrical behavior, the side to which its majority charge carriers flowing to would be hot. If n-type and p-type semiconductors are biased in the same direction, their charge carriers flow in opposite direction. As a result, n-type and p-type Peltier elements create opposite temperature gradients when

biased in the same direction as shown in following figure:

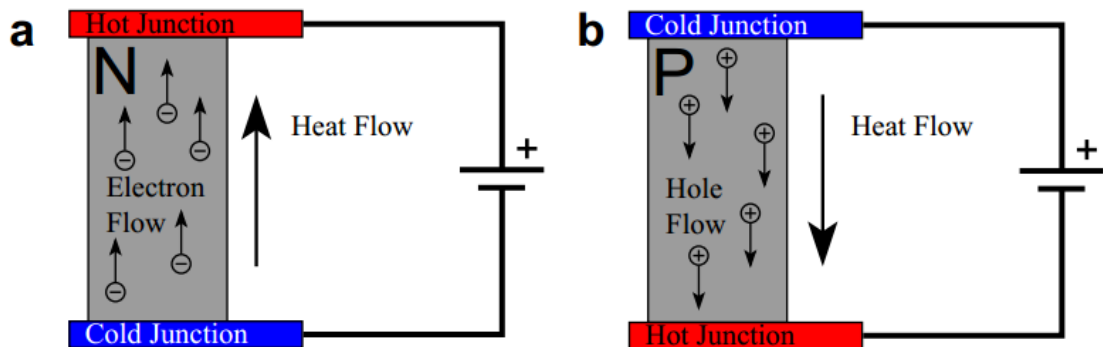


Figure 5.2 N-type and P-type Peltier Elements

For a single Peltier element, the heat produced or removed is generally not sufficient for realistic situations. Commercial Peltier devices are composed of many n-type and p-type semiconductor Peltier elements to increase the heat generating (or removing) power. The individual elements are connected in series using metallic junctions like copper that both have good electrical and thermal conductivity. As shown in following figure the heat flow is in the same direction:

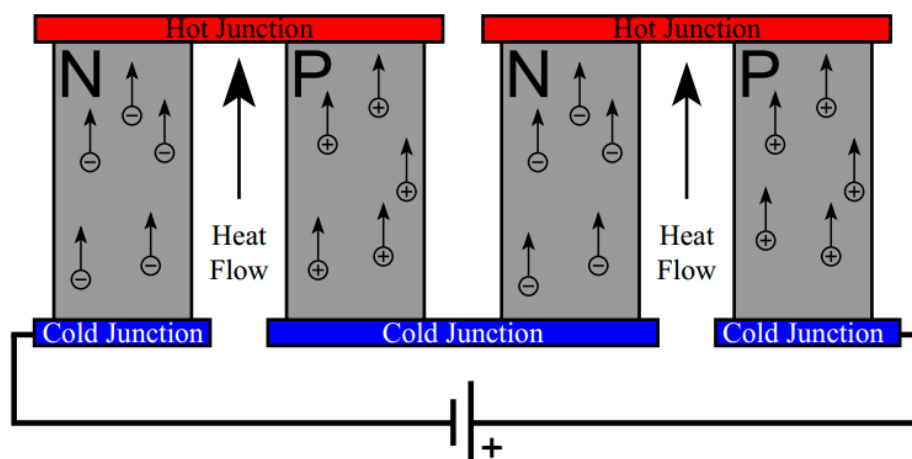


Figure 5.3 A Series of Alternating N- and P-type Semiconductor Elements

A complete Peltier device composition is shown in figure 5.4. It consists of two insulating ceramic plates sandwiching a series of p-n pairs joined by copper. This

design provides a large surface area improving heat pumping for cooling and heating applications.

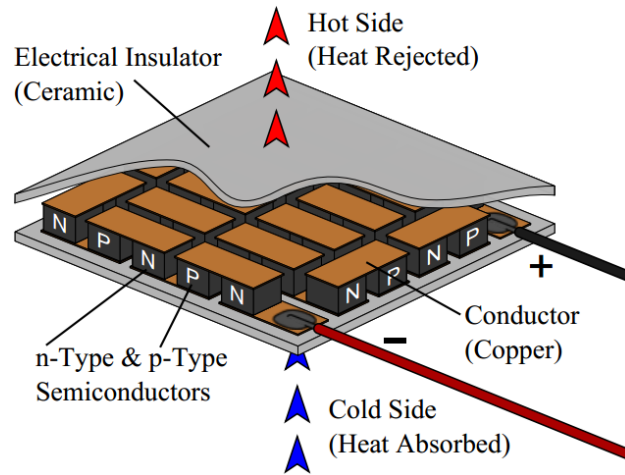


Figure 5.4 Design of a Commercial Peltier Device

Although low in efficiency, Peltier element based temperature controllers offer many advantages, they are accurate and easy to adjust and can stay stable for a certain desired temperature which is ideal for our application. I tried to build a temperature chamber by myself, but this is a big project already and thermal insulation is not guaranteed. There are commercial refrigerator/heaters on the market, some of them can adjust temperature from -10° to 60° Celsius. That's enough for the experiment temperature range. So we bought a temperature chamber with the precision of temperature control to 1° , it only cost about 50 dollars and the insulation is guaranteed. If one wants to build a temperature chamber, the dedicated Peltier elements can cost 200 dollars already.

5.2 Sampling System

Now that we have temperature chamber ready, we can build the whole calibration system. It is shown in the following figure, a valve control the overall flow rate of

ultra-purity nitrogen gas. The sampling tube then split into two parts, one of them flow through a water container, by adjusting the flow meter on each flow branch we

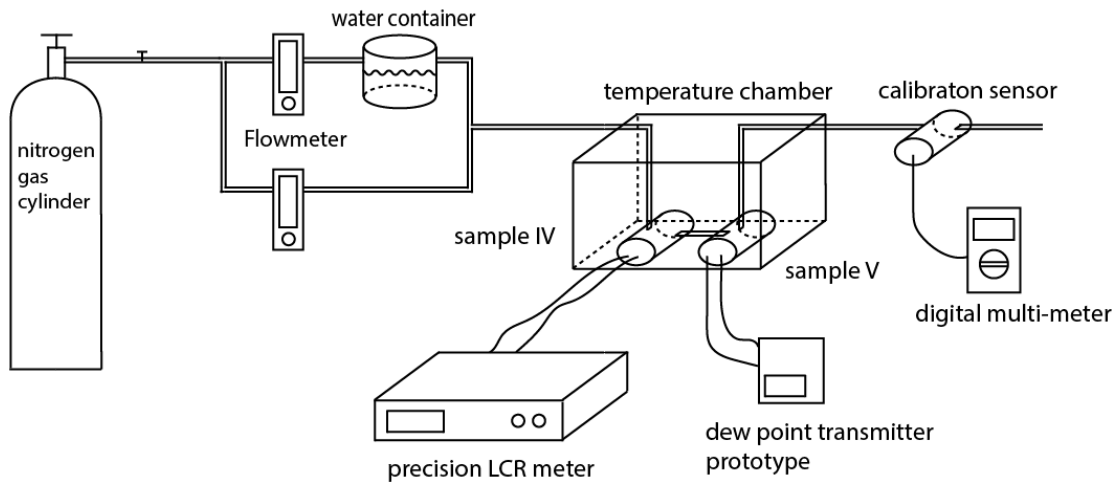


Figure 5.5 Illustration of Calibration Sampling System

can control the humidity level of the air flowing through sample IV sensor. In order to insert the sampling tube inside the temperature chamber, two holes were drilled on top of the chamber. The diameters of these holes are about the same of that of the tube, this ensures heat insulation. We have two humidity sensor placed inside the temperature chamber, one is sample IV and the other is sample V, both of them are installed inside dedicated testing chambers made from steel. They are connected by sampling tube, which allows sampling air to go through.

A precision LCR meter monitor sample IV's resistance and capacitance. The temperature sensor mentioned above is positioned next to sample V in the testing chamber. Both the temperature sensor and the humidity sensor sample V are connected with our dew point transmitter prototype described above. The sampling tube then guide the airflow into calibration sensor chamber, a digital multi-meter

reads the instant current reading. We can calculate dew point based on current reading.

The sampling tubes are made from hard plastic Teflon, stainless steel is a good alternative in the future.

There is something worth saying about the temperature chamber. Although it has a segment display that tells you the temperature, but actually the value shows is the instant surface temperature of Peltier element as well as that of the wall in the chamber. The temperature sensor in testing chamber gives the real temperature of humidity sensor, we can observe it on the LCD module. By observation, the program in control panel of the Peltier element is set that it begin to work when the actual temperature deviates the set temperature 2 °C. So when setting the temperature, we should set it 2 °C opposite direction the room temperature. For example, the room temperature is 23 °C, if we want test the humidity sensor at 10 °C, 8 °C is actually set. When surface of Peltier element reaches 8 °C, it stopped then because room temperature is high than 8 °C, it will slowly warm up until 10 °C it will work again and pretty soon the surface come back to 8 °C. This process goes back and forth, after running for a long time, and takes thermal insulation imperfection into consideration, we will get the desired temperature at humidity sensor.

Chapter 6 Experiment Results

Test experiments are being conducted using the calibration sampling system mentioned above. Two humidity sensors were under test in the lab, they were produced at the same time using the same technique. So they basically are the same although some minor difference may remain. Sample IV acted as the reference sensor, the probes from a precision LCR meter (model type Agilent 4284A) is connected to the four input terminals of this sample, so we can monitor the capacitance and resistance change under different humidity and temperature levels. They are both fundamental physical properties that typically measured to reflect humidity sensor's behavior. Sample V works with the dedicated transmitter prototype, the separated board will connect to sensor chamber directly without wires, and they are put in the temperature chamber together. After the experiments the "circuit reading" can be related to dew point values. And further modeling will go from there.

The calibration reading were given by a commercial dew point sensor FA410-H2 manufactured by CS Instruments, we'll see later in experiment results that this sensor has some flaws, especially at low dew point range. Although this may make no difference in modeling methods it sure would affect the accuracy of modeling results. And it is an empirical (secondary measurement) device, meaning it measure a change in some material as a relation to humidity, it does not measure any fundamental property of water vapor. To meet commercial level standards, a precise chilled mirror hygrometer is needed in the calibration process.

It is not feasible to make measurement of sensor readings of all possible dew points

under 51 different temperatures. It is time consuming and low in efficiency. The strategy behind calibrating this humidity sensor is to record the circuit readings under different humidity of a few temperatures and then develop a model so we can interpolate circuit reading of other temperatures. According to former experience, for a given temperature, the dew points and testing time are given below:

Table 6.1 Dew Point Test Points

N2(lit/min)	H2O(lit/min)	FA410(mA)	DP(°C)	Time
0	~800	~19.5	~18	30(min)
~750	~600	18.23	8.9	30(min)
~1100	~300	16.80	0	30(min)
~1100	~200	15.68	-7	1(hr)
~1100	~40	13.28	-22	1(hr)
~1100	~10	11.07	-34	1(hr)
~1100	~5	9.0	-50	1(hr)
~1100	~0	More dry	More dry	1(hr)

In high humidity range the testing time is half an hour, for lower dew points the testing time become one hour which allows more time for the sensor to give a more reliable value. The testing temperatures are from 0 °C to 50 °C with 10 °C intervals. So a total of 6 temperatures were tested. In order to take hysteresis into consideration, the nitrogen gas will run at the last setting overnight and in reverse order test other dew points. For those tested temperatures below room temperature, the highest dew points

tested are controlled to be about 2 degrees below that temperature. This is to prevent the actual dew or ice (at 0 °C) to be formed on the surface of humidity sensor. Because if that happens, the property of humidity sensor may be changed and give erratic readings.

For illustration purpose, test results at temperature 30 Celsius will be presented and discussed, the results of other temperatures are about the same. The following two figures show the sensor capacitance and circuit reading changing with time at 30 °C respectively.

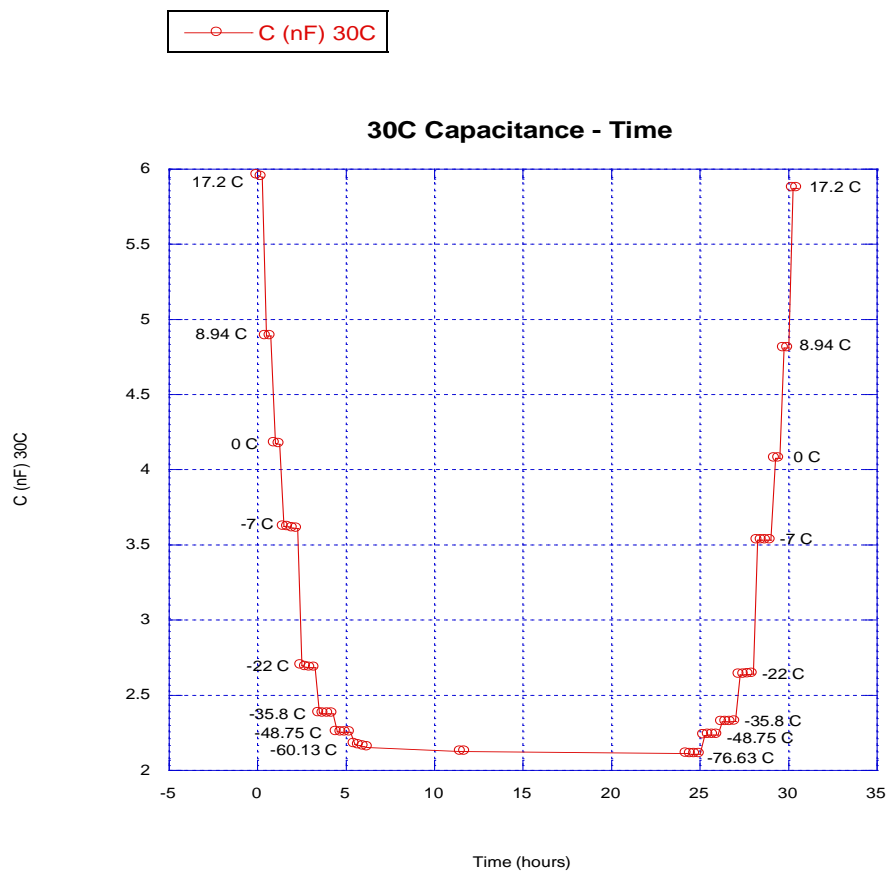


Figure 6.1 Sensor Capacitance vs. Time at 30 °C

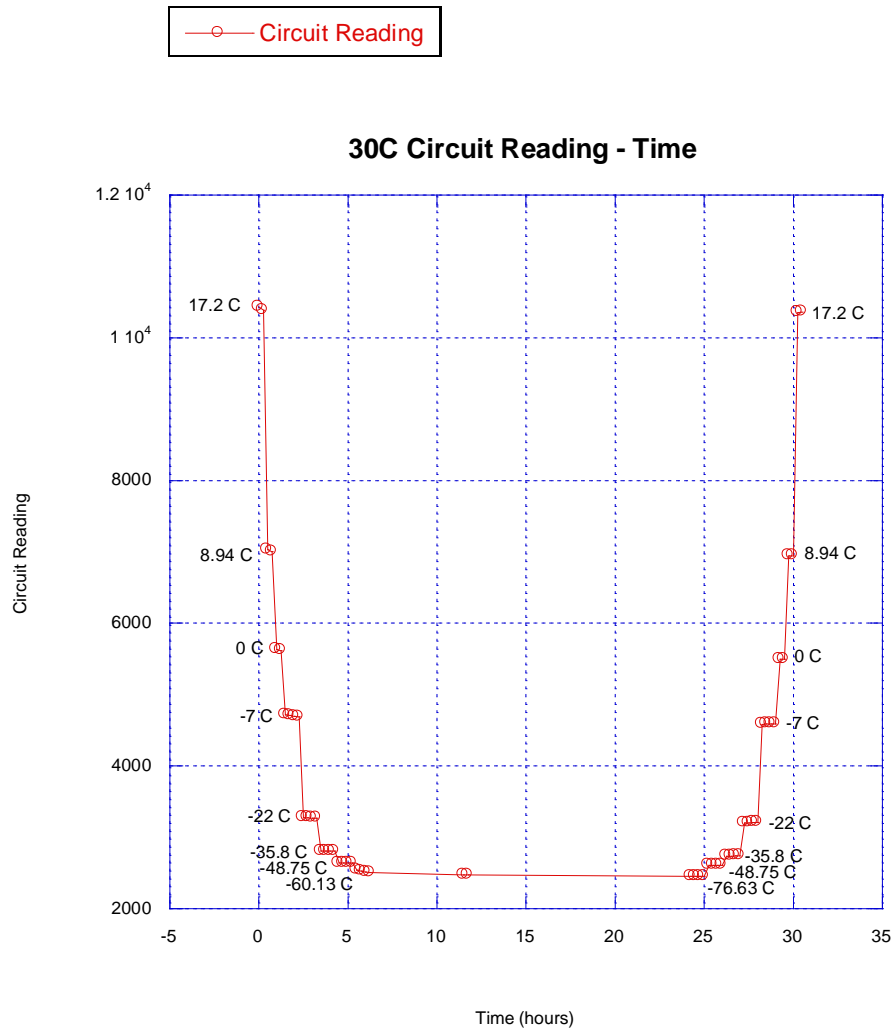


Figure 6.2 Sensor Circuit Reading vs. Time at 30 °C

They have the same shape because the circuit reading is actually a digital representation of sensor capacitance. Noticed that at lower dew points there are more recording times, that's because more time are allowed for stability at lower dew point. During each day of the measurement, the data were taken down every 15 minutes. Those two figures give us an overview of how the experiment of a particular temperature is conducted.

The following figure shows dew point vs circuit reading, it include all the tested points in two days experiment of a given temperature. This figure is the most

important and useful one, it shows relation between dew point and circuit reading, adjacent dew points are connected by straight lines, gives us a feeling of how circuit reading changes with dew point. But the data falls in between sure is not accurate enough, more advanced curve fitting technique will be discussed in next chapter.

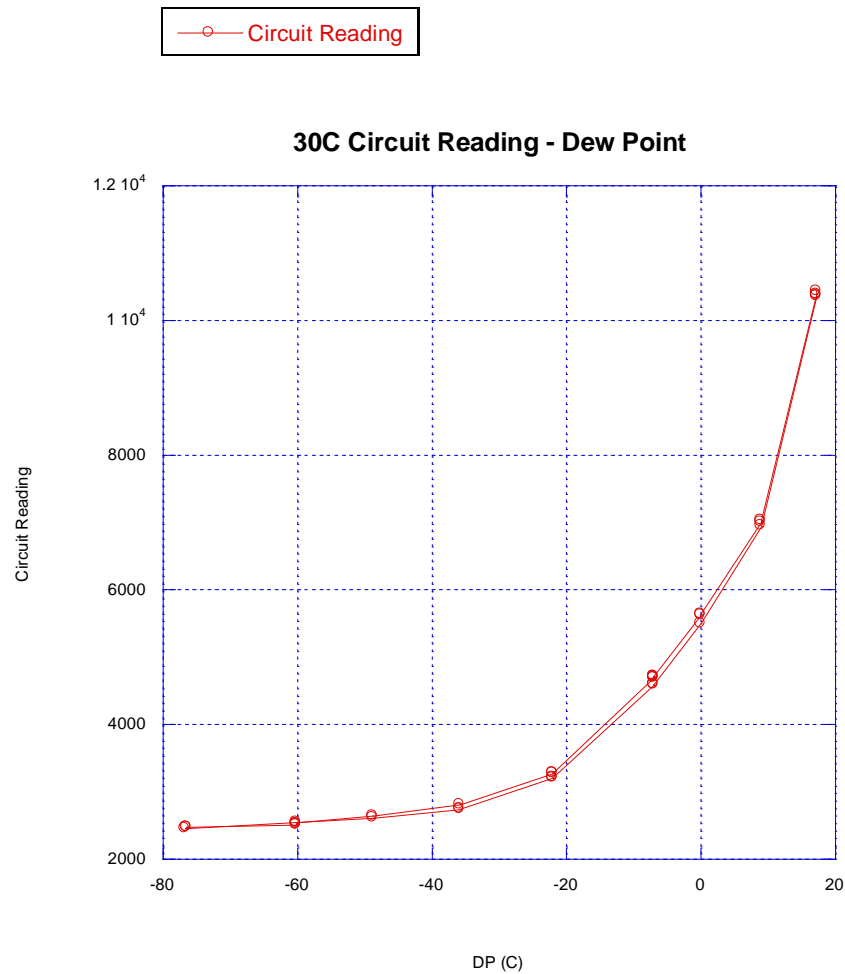


Figure 6.3 Circuit Reading vs. Dew Point at 30 °C

Note that the two day's readings of a given dew point do not completely overlap, the first day's reading is a little higher than that of the second day. This is due to the intrinsic hysteresis property of the humidity sensing material. Before the experiment, the humidity sensor had been exposed in the open atmosphere with high humidity

level for a long time, not only adsorption occurred, but there was chemisorption. The humidity sensor needs more time during desorption to get rid of water molecules formed by chemisorption, that's why we get lower readings the next day. Hysteresis is unavoidable in all empirical sensors, it is a good thing that this humidity sensor shows little hysteresis phenomenon, which make it more capable of giving reliable readings. To compensate hysteresis, we can simply use the average value of two day's readings. If we zoom in the figure in the lower humidity range, we noticed that the dew point transmitter FA410 (CS Instrument) gave flawed readings at around -60 °C. When the actual humidity level is

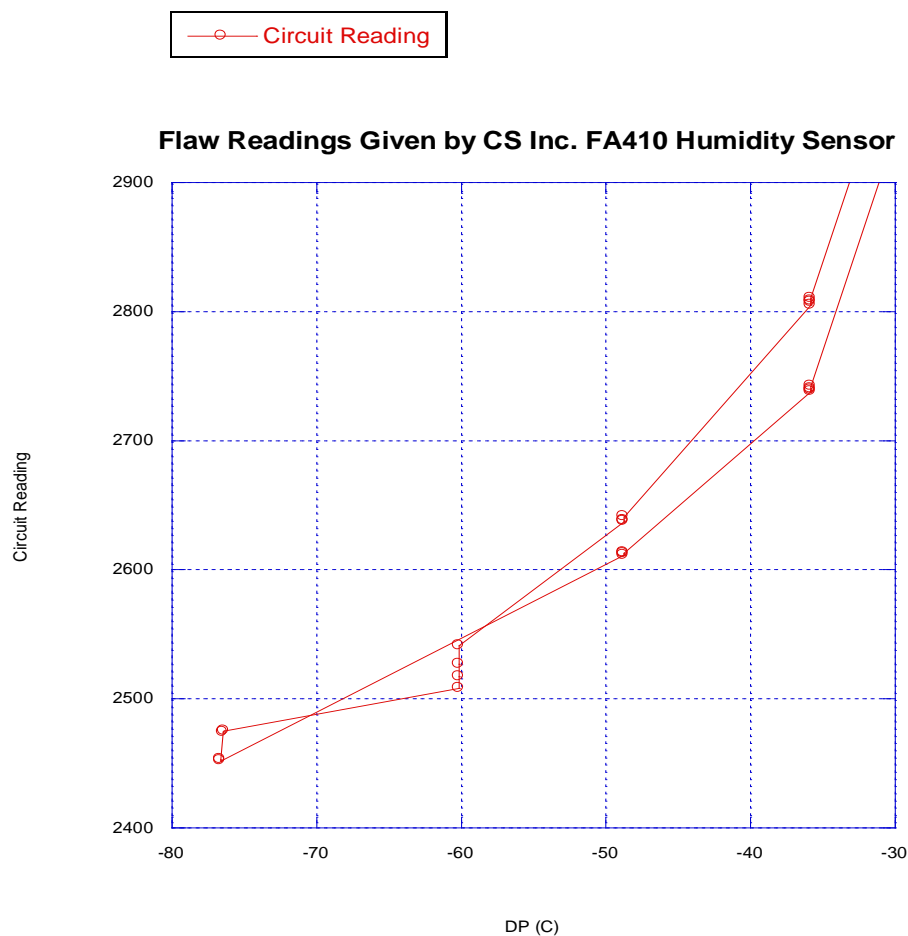


Figure 6.4 Flaw of CS Instrument's Humidity Sensor

decreasing, which is shown by lowered readings, the FA410 kept output the same dew point. This can be the sensor's incapability of sensing ultra-low humidity level, or more probably the flaw within the sensor circuit or program. Either one makes it a not very good humidity transmitter. For real humidity calibration, this FA410 humidity sensor is barely usable. But for the time being, we can at least utilize it to do research of further modeling methods. When doing the data modeling, the flawed data will be eliminated.

The figure below shows all the dew point/Reading relations all together.

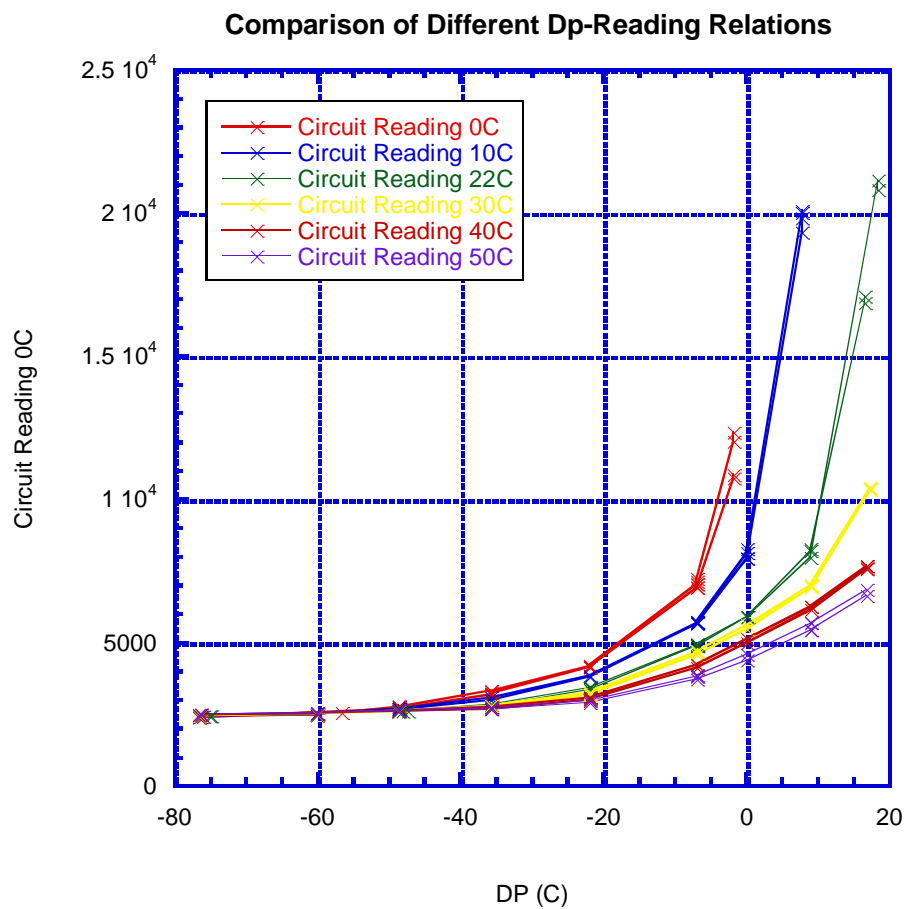


Figure 6.5 Comparison of Different Dew Point/Reading Relations

The figure above shows all tested dew point and reading relations. We can see that for very lower dew points (dew point $< -50\text{ }^{\circ}\text{C}$), the circuit readings under different temperatures are about the same, and there isn't much difference. But at higher dew point range, if the temperature is higher, the circuit reading would be lower. We can almost feel the changing trend, careful modeling methods are discussed next chapter to get all those data points in between these lines.

Chapter 7 Temperature Compensation Modelling

With the valuable experiment data obtained, the next and the most important step is data modeling. The problem is how to get all the other dew point – temperature – circuit reading points as accurate as possible. In mathematical field of numerical analysis, interpolation is a method of constructing new data points within the range of a discrete set of known data points.

After getting median readings of a same dew point and eliminating the false readings we get those datasets that can then be used for data modeling. The following table shows all the datasets:

Table 7.1 Modeling Points

0 °C		10 °C		22 °C	
DP	Reading	DP	Reading	DP	Reading
-1.88	11500.5	7.6875	19828.25	18.34	20982
-7.00	7034.5	0	8090.5	16.5	17000
-22.00	4187.5	-7	5704.1	8.9375	8116.75
-35.81	3278.9	-22	3840	0	5916
-48.75	2744.8	-35.812	3052.9	-7	4927.6
-56.63	2570	-48.75	2688.9	-22	3409.5
-76.63	2403	-76.688	2426	-35.812	2811.1
				-48.75	2616.6
				-76.688	2430
30 °C		40 °C		50 °C	
DP	Reading	DP	Reading	DP	Reading
17.25	10385	16.75	7646.75	16.75	6752.75
8.94	6980	8.94	6223	8.94	5584.75
0.00	5560.5	0.00	5072.25	0.00	4504
-7.00	4646.1	-7.00	4193.9	-7.00	3794.4
-22.00	3242.1	-22.00	3063.9	-22.00	2951
-35.81	2773.6	-35.81	2725.4	-35.81	2716.5
-48.75	2625.1	-48.75	2627.4	-48.75	2633.4
-76.63	2452	-76.69	2481	-76.69	2503

It's not difficult to find out that this turns out to be a multivariate interpolation problem, when you need more than one variable to determine and get the output or interpolated value. For this problem specifically, a temperature and a dew point will correspond to a single circuit reading. If we picture it using a 3D model, the datasets are actually points in it whose three axes represent dew point, ambient temperature, and circuit reading.

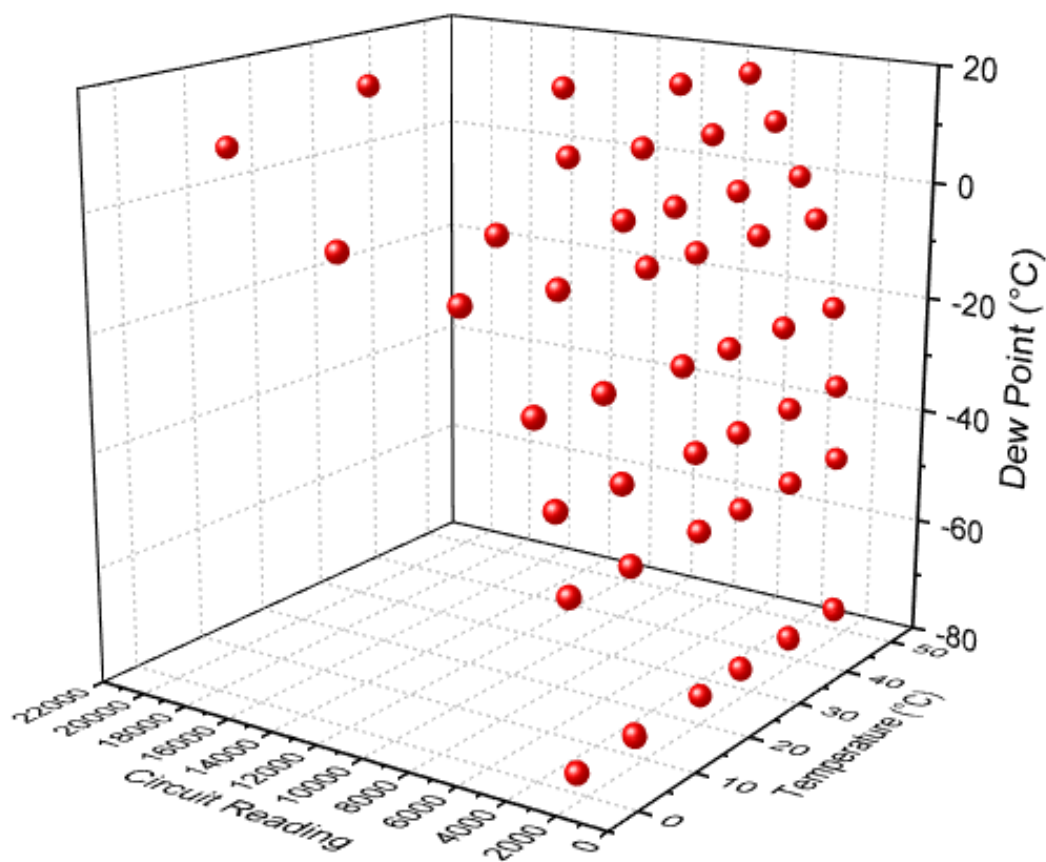


Figure 7.1 3D Scatter Plot of Datasets

7.1 Two Dimensional Analysis

7.1.1 Linear Interpolation

Remember in last chapter, for the curve of dew point and reading relationship of a specific temperature, the data points are connected by straight lines. This used the

method of linear interpolation. It is one of the simplest interpolation methods, for two data points on a plane (x_a, y_a) and (x_b, y_b) , at point (x, y) the interpolant is given by:

$$y = y_a + (y_b - y_a) \frac{x - x_a}{x_b - x_a}$$

Linear interpolation is quick and easy, but it is not very precise, the error is smaller when the distance between data points gets smaller.

7.1.2 Polynomial Interpolation

Given n points in a plane, $(x_k, y_k), k = 1, \dots, n$. with distinct x_k , there is a unique polynomial in x of degree less than n whose graph passes through the points. This polynomial is called the interpolating polynomial. The interpolant is a polynomial so thus infinitely differentiable. Although it is smoother than linear interpolation, it also has some disadvantages. It is computationally expensive compared to linear interpolation and furthermore it may exhibit oscillatory artifacts especially at end points, this is known as Runge's phenomenon in numerical analysis. This makes polynomial interpolation not quite usable in engineering problems.

7.1.3 Piecewise Cubic Interpolation

Many more effective and accurate interpolation techniques are based on piecewise cubic polynomials. MATLAB has two different functions for piecewise cubic interpolation, `spline` and `pchip`. Spline is the most famous member in the piecewise cubic polynomial family. All piecewise cubic polynomials are continuous and have a continuous first derivative, a spline however is exceptionally smooth, its second derivative is also continuous [35]. The function `pchip` actually stands for shape

preserving piecewise cubic Hermite interpolating polynomial. This function is not as smooth as spline, there may be jumps in the second derivative. It is designed so that it never locally overshoots the data, this makes it very useful for many real world problems [36]. Pchip is local, the behavior of pchip on a particular subinterval is determined by only four points, the two data points on either side of that interval. It is unaware of the data farther away. Spline is global, the behavior of spline on a particular subinterval is determined by all of the data. Below is a figure of different interpolation methods responding to a unit impulse.

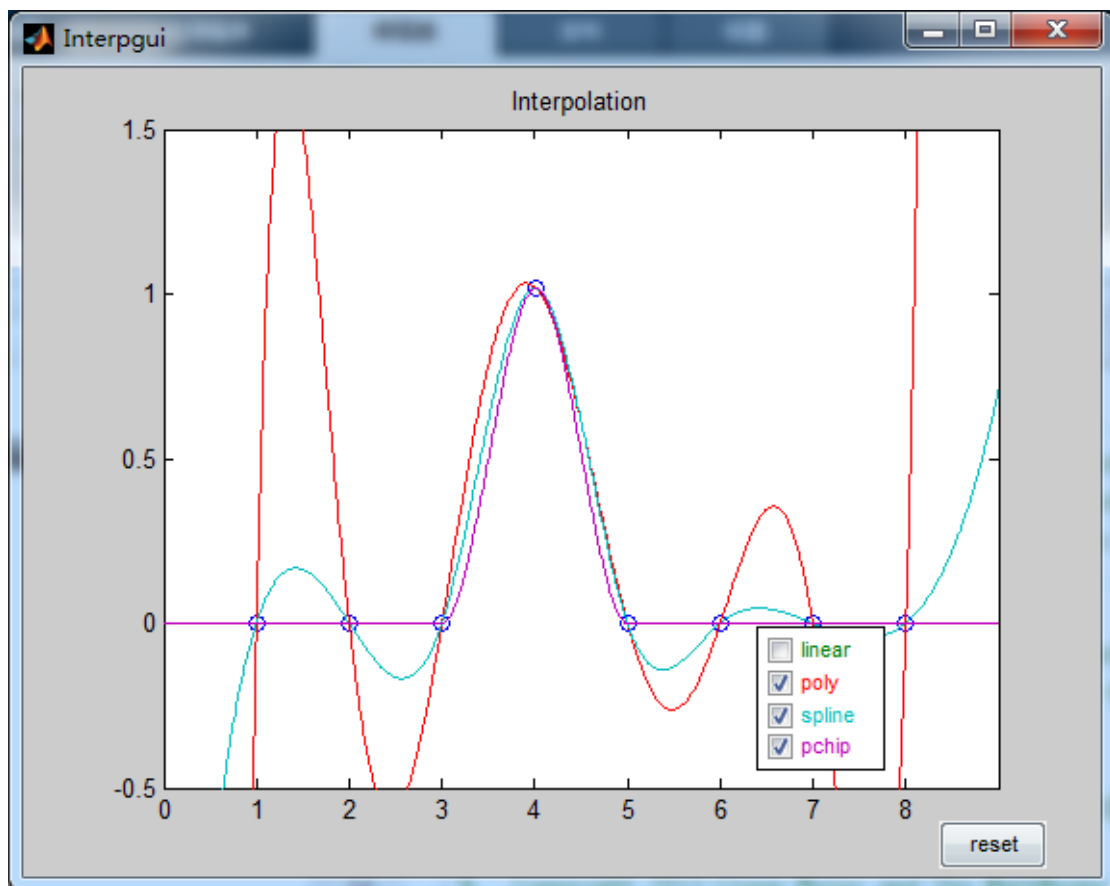


Figure 7.2 Comparison of Different interpolation Methods to an Impulse

Noticed in the figure that the support of pchip is confined to the two intervals surrounding the impulse, while the support of spline extends over the entire domain.

The polynomial interpolation is simply too oscillatory. The following eight subplots spline and pchip on a slightly larger data set.

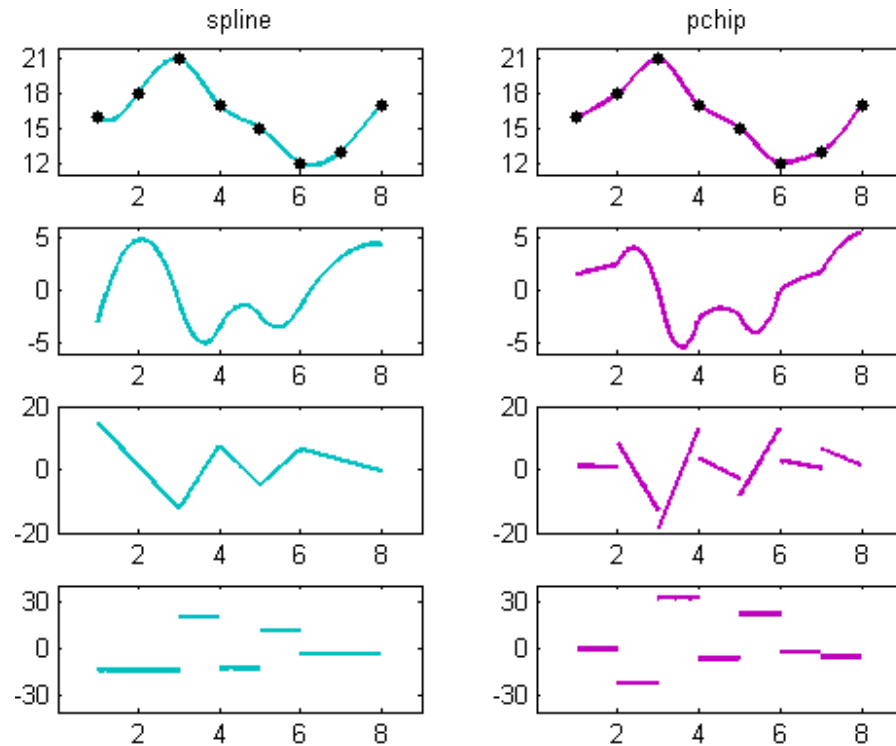


Figure 8.3 Spline Vs Pchip

The first two plots show the function $s'(x)$ and $p'(x)$, the difference between these two interpolants is barely noticeable. The next two plots show the first derivatives, they are both continuous but $s'(x)$ is smoother than $p'(x)$. The third pair of subplots show the second derivatives, $s''(x)$ is continuous but $p''(x)$ jumps at sample points. The final pair are the third derivatives. Because both functions are piecewise cubic polynomials, their third derivatives $s'''(x)$ and $p'''(x)$, are piecewise constants.

Here are some difference between spline and pchip [37]:

- Spline produce a smoother result
- Spline produce a more accurate result if the data consist value of a smooth

function

- Pchip has no overshoots and less oscillation if the data are not smooth
- Pchip is less expensive in calculation

Below is a figure of different interpolation methods used to interpolate circuit readings at 30 °C:

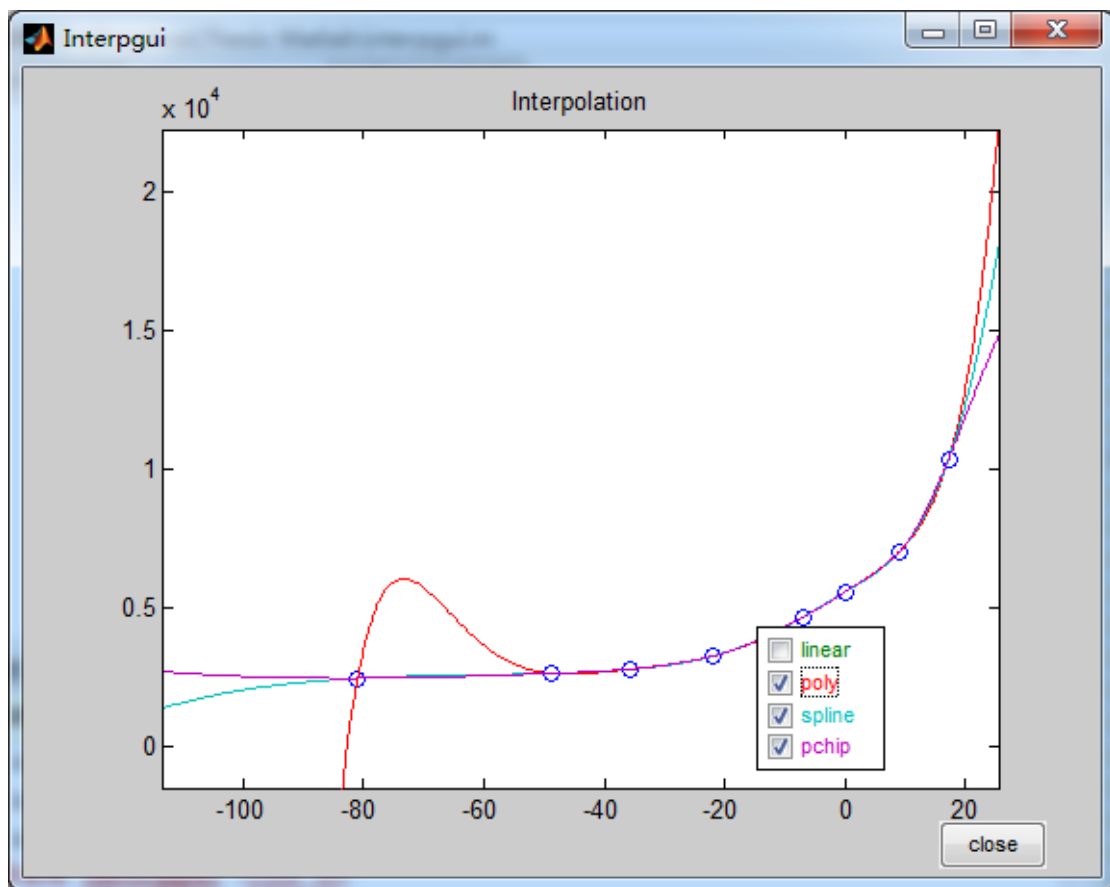


Figure 7.4 Comparison of Different Interpolants Using Dataset at 30 °C

Again the polynomial interpolation is too oscillatory at end points. The difference of spline and pchip between the data points is barely noticeable, however the extrapolation of spline at high dew point range seems more accurate than pchip. For low range dew point extrapolation, we can use linear interpolation.

7.2 Three Dimensional Analysis

Matlab offer the function `interp2` for 3 dimensional interpolation and extrapolation, the syntax is `Vq = interp2(X, Y, V, Xq, Yq, method)`. It has four methods, 'linear', 'nearest', 'cubic', and 'spline'. X, Y are sample grid points specified as matrices or vectors, if X and Y are matrices, then they contain the coordinates of a full grid, a full grid is a pair of matrices whose elements represent a grid of points over a rectangular region. If X and Y are vectors, then they must be strictly monotonic and increasing. For this dew point modeling problem, because different temperatures may have different number of readings, so the function `interp2` cannot be used here. The Matlab function "griddata" is actually for this kind of scattered data interpolation, but the results are not acceptable. We can create an interpolation script using existing Matlab functions for this problem specifically. The algorithm is introduced in following sections, and it extends the use of `pchip` to 3 dimensional interpolations.

7.2.1 Artificial Neural Networks Method

A more advanced method for data fitting and pattern recognition is using ANN or artificial neural networks. A neural network consists of neurons, grouped in layers. The most commonly used ANNs are feed-forward networks. The following figure shows the structure of a neural network:

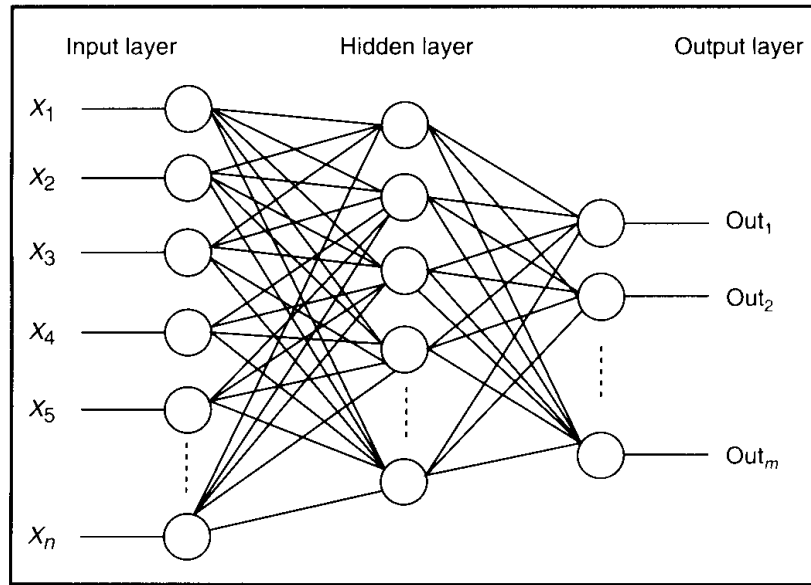


Figure 7.5 General Structure of a Neural Network

Matlab has a very easy to use neural networks tool box that support several usages.

For example, curve fitting and pattern recognition. To work with neural networks

curve fitting app in Matlab, the sequence of the training process is as follows:

1. Feed the neural networks with inputs and outputs, in this case the inputs are dew points and corresponding temperatures, the outputs are circuit readings. The dew points and temperature are combined to form a 47×2 matrix, the neural networks tool box has no limitation for matrix or vector monotonicity.
2. Chose the percentage of validation data and testing data, the default setting is training data takes 70%, validation data and testing data take 15% respectively. Validation data are used to measure network generalization, and stop training when generalization stops improving. Testing data have no effect on training and used to measure the network performance during and after training.
3. Chose the number of hidden neurons. The standard network that used for function

fitting is a two-layer feed forward network, with a sigmoid transfer function in the hidden layer and a linear transfer function in the output layer. The default number of hidden neurons is set to 10. This number can be increased later if the network training performance is poor. The following graph show the implemented neural network:

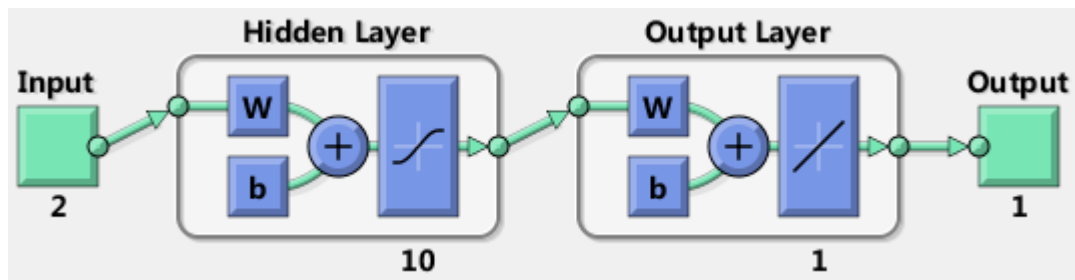


Figure 7.6 Implemented Neural Network Diagram

4. Select a training algorithm, the default is Levenberg-Marquardt algorithm and is recommended for most problems. For some small and noisy problems Bayesian Regularization can take longer but obtain a better solution. For larger problems, Scaled Conjugate Gradient is recommended as it uses gradient calculations which are more memory efficient than the Jacobian calculations the other two algorithms use.

After training using a specific algorithm, the training result is shown. The MSE stands for mean squared error is the average squared difference between outputs and targets. Lower values are better. Zero means no error. The Regression R values measure the correlation between outputs and targets. An R value of 1 means a close relationship, 0 is random relationship. All three algorithms are used to train this problem, or some reason however, no satisfactory results were given, the errors are exaggeratingly big.

No matter how many times you retrain the network, the scale of error still cannot be reduced. The results for three different algorithms are shown below:







	 Samples	 MSE	 R
 Training:	33	417.94664e-0	9.99991e-1
 Validation:	7	261583.25906e-0	9.74766e-1
 Testing:	7	97575.52390e-0	9.97450e-1

Figure 7.7 Sample Results Using Levenberg-Marquardt Algorithm







	 Samples	 MSE	 R
 Training:	33	14.89635e-0	9.99999e-1
 Validation:	7	0.00000e-0	0.00000e-0
 Testing:	7	112374.39281e-0	9.98030e-1

Figure 7.8 Sample Results Using Bayesian Regularization Algorithm







	 Samples	 MSE	 R
 Training:	33	416920.28567e-0	9.87370e-1
 Validation:	7	25391.21149e-0	9.73392e-1
 Testing:	7	3534096.18601e-0	9.75997e-1

Figure 7.9 Sample Results Using Bayesian Regularization Algorithm

The number of neurons in the network was increased, the retraining takes much longer but the results are still not good. I've also tried to increase the percentage of training data, but this also didn't work. The only way possibly to reduce error is to provide the network with a bigger data set, especially when the inputs are more than one. The training data were just too few for existing neural networks algorithms to produce an accurate result. However, Acquiring more input datasets are time inefficient. Those neural networks algorithms are general purpose algorithms, so they are less that powerful when not enough training data are provided. Humans have billions of real neurons and are not confined to little number of algorithms, in the

model presented in figure 8.1 we can almost feel the tendency of the surface. It is possible to design a dedicated algorithm to produce very accurate results.

7.2.2 3-D Delaunay Triangulation

Another possible method for 3 dimensional data fitting is by creating triangular surfaces of the data points. The following is a wired surface graph generated by origin pro, and it uses Delaunay triangulation. Delaunay triangulation can be used to create a continuous surface from a set of data points by creating a triangular mesh or surface of triangular planes connecting the data points. Delaunay triangulation is considered to be a desirable approach for creating natural-looking surfaces because minimum interior angles of all triangles are maximized and triangles are as equiangular as possible, so long, thin triangles are avoided.

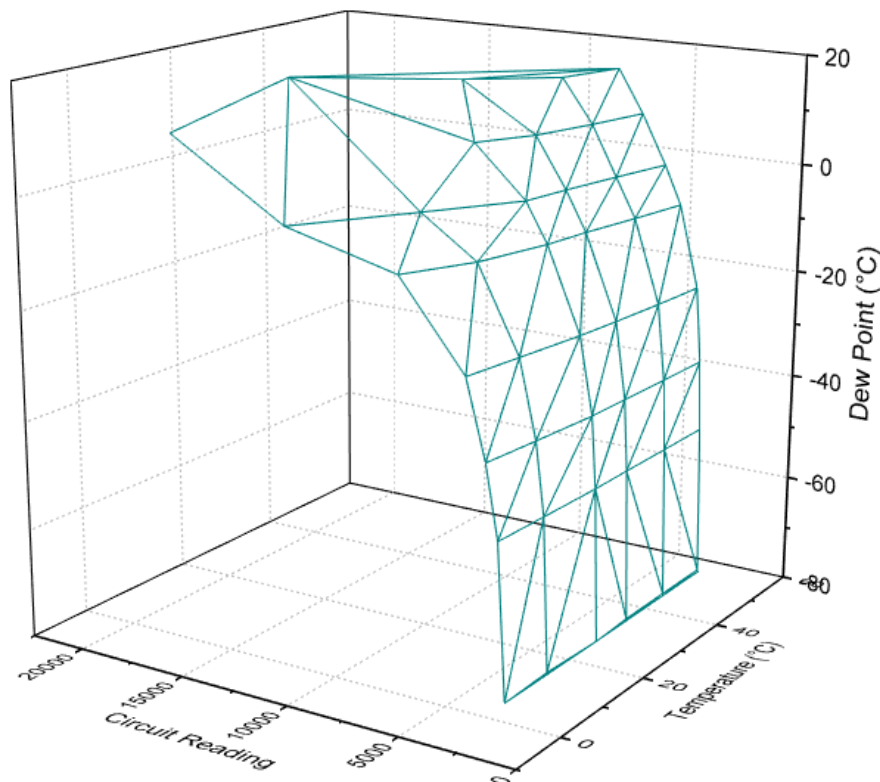


Figure 7.10 Delaunay Triangulation Wired Surface of Data Points

Because we know each point on each of these triangles, it's not hard to get all other points on that triangle surface. The circuit readings are more "sensitive" to dew point at lower humidity range, a little change in circuit reading will change the dew point. If you get a section view of the graph by this method, you'll actually see a zigzag shape of line. If x is one particular dew point and $\text{Reading}(x)$ is the corresponding circuit reading, for a good interpolation of our humidity sensor application, the interpolated curve of dew point and circuit reading relation under a certain temperature should conform to the following rules:

1. The curve passes through all sample data
2. $\text{Reading}(x+1) > \text{Reading}(x)$
3. $\text{Reading}(x+1) - \text{Reading}(x) > \text{Reading}(x) - \text{Reading}(x-1)$

For the above algorithm, it does not obey rule 2 and 3, so it is not good and not suitable for our application. Although we can't use this method directly, it inspired me to design my own interpolation algorithm. The interpolation through Delaunay triangulation is like using linear interpolation in multiple planes. In earlier section we've seen how well the `pchip` function in Matlab did in 2 dimensional interpolations. Basically the following implemented algorithm is using `pchip` function in multiple planes.

7.2.3 An Algorithm for Sensor Temperature Compensation

The algorithm is implemented using Matlab. First use `pchip` function on the circuit reading and dew point relation of all 6 tested temperatures. For convenience of

modeling, I used $-81\text{ }^{\circ}\text{C}$ as the lowest dew point, later experiments shows that this is more close to the actual dew point which is $-82\text{ }^{\circ}\text{C}$. This is the reason why empirical sensors should not be used for calibration, it's not accurate. Those interpolation curves are generated directly from sample points so we assume they are the most accurate ones, we can further construct the surface using all the points on these curves. Because the circuit readings were measured at the same dew points of all tested temperatures, if we fixed the dew point value, we can get relation of circuit reading and temperature of one particular dew point. We can round the tested dew points to the following integers $-80\text{ }^{\circ}\text{C}$, $-49\text{ }^{\circ}\text{C}$, $-36\text{ }^{\circ}\text{C}$, $-22\text{ }^{\circ}\text{C}$, $-7\text{ }^{\circ}\text{C}$, $0\text{ }^{\circ}\text{C}$, $7\text{ }^{\circ}\text{C}$, $9\text{ }^{\circ}\text{C}$, $17\text{ }^{\circ}\text{C}$. For those dew points above $0\text{ }^{\circ}\text{C}$, the number of sample data is smaller. For illustration purpose, the interpolation at dew point $0\text{ }^{\circ}\text{C}$ using pchip is shown below:

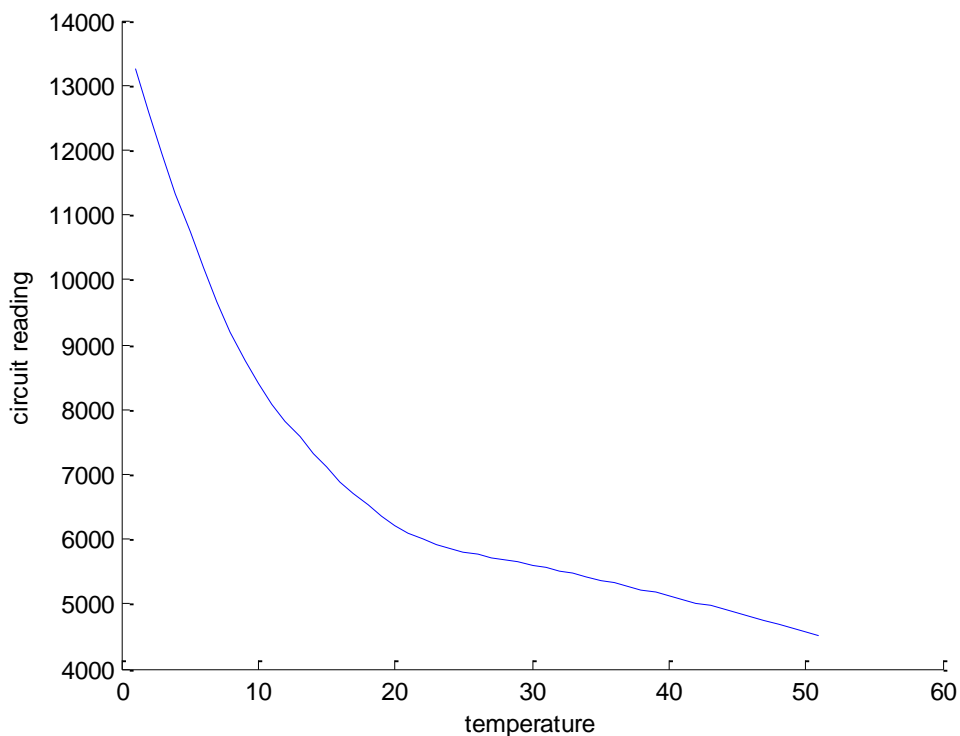


Figure 7.11 Relation of Temperature and Circuit Reading at $0\text{ }^{\circ}\text{C}$ Dew Point

We can then do this with other dew points. Then the interpolation of dew point and reading relation from temperature 17 °C to 49 °C are made also using pchip. For those between sample temperatures, previously interpolated values are used for further interpolation. The reason why started from temperature 17 °C here is that the readings at dew point 17 °C can now be used here, and for above 20 °C temperatures, the highest dew point keeps constant to be 20 °C, the extrapolation range is small to keep the accuracy. The interpolations below temperature 17 °C need a bit more work. From here the highest dew point under a temperature is the same as the temperature. We can first get that highest dew point circuit reading by extrapolate 1 °C temperature below all those previously interpolated readings. For example, if I want to get interpolation of dew point and reading relation at temperature 16 °C, I want to know the circuit reading at highest dew point, which is also 16 °C. The circuit reading at dew point 16 °C is already interpolated through all those previously interpolated temperatures above 16 °C, so we can just extrapolate 1 °C temperature below to get the circuit reading of dew point 16 °C at temperature 16 °C. The interpolation at temperature 16 °C can be made. The process goes on and on until the interpolation under temperature 1 °C. It's like weave the surface back and forth from two planes using pchip. Below is the final result, the figure contains 4941 points:

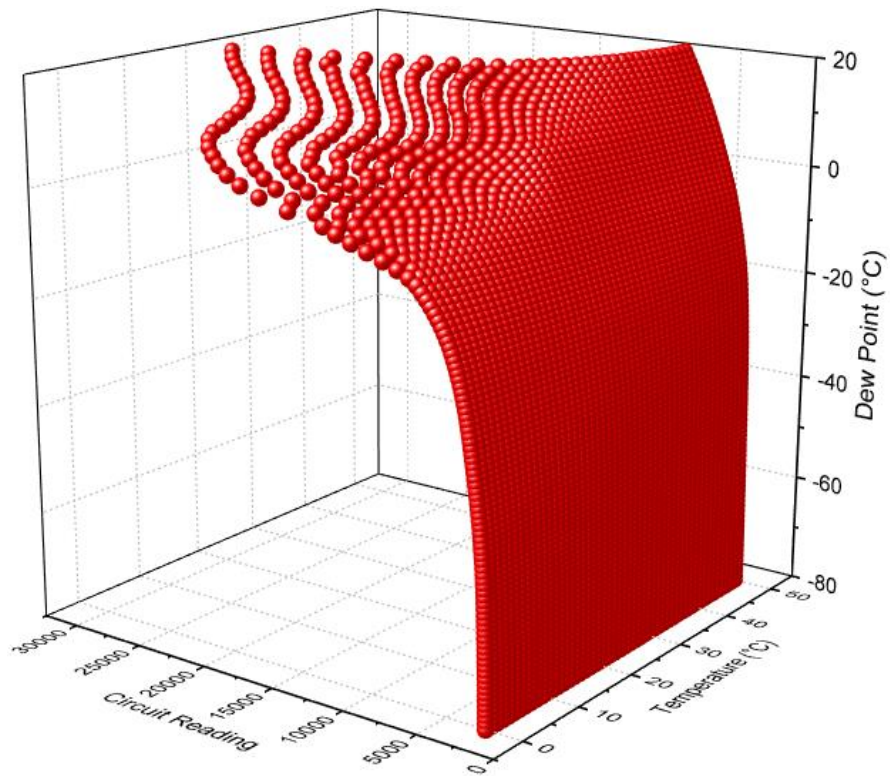


Figure 7.12 Results after Implementing the Algorithm (1)

If switch the parameter of the axes, the following graph is more familiar:

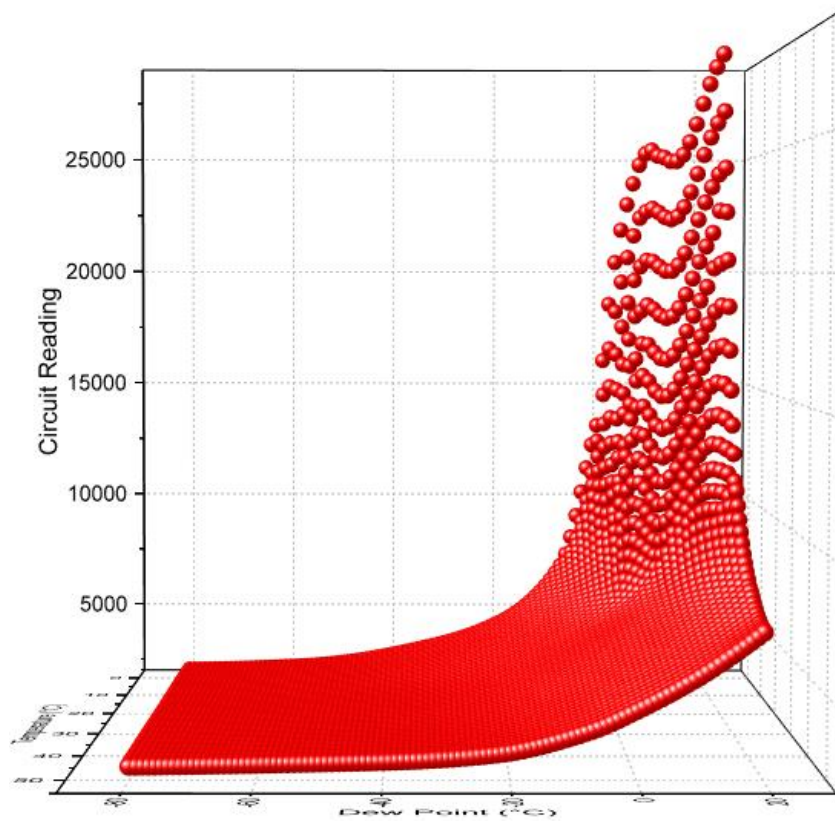


Figure 7.13 Results after Implementing the Algorithm (2)

We can see the result of using this dedicated algorithm is much better and smoother than the previous ones. Noticed the big space between those high humidity readings, this means that the tolerance for error is much bigger than those of very low humidity.

7.2.4 Embedded Code Implementation

Now that we get all the reading of different dew points under different temperatures, we can now implement code working with other modules to get dew points. The reading data is stored as matrix or 2-D array in the flash memory of memory MSP430. The indexes of the first dimension indicate temperatures, and indexes of the second dimension indicate the dew points. The algorithm is fairly easy, a function was written to take two arguments, one is temperature, the other is circuit reading, the reading was compared with the readings of an array corresponding with the temperature, and the function returns the dew point value.

Chapter 8 Conclusion and Future Work

8.1 Conclusion

The dew point meter described in this thesis is based on an alpha-alumina-based humidity sensor, which is a drift-free humidity sensor. Experiments of the sensor showed great performance of long time stability and reliability. A prototype of a humidity meter was developed using slope A/D conversion technique. The embedded system based on MSF430 microcontroller was improved for better performance. The sensor showed very good capability of measuring very low humidity.

The Peltier effect temperature chamber offered an affordable way of controlling the temperature between range of $-5\text{ }^{\circ}\text{C}$ to $60\text{ }^{\circ}\text{C}$, the capacitance of the humidity sensor was tested under different temperatures and different humidity levels. After collecting the data points, several interpolation methods were studied. Neural networks is also a good tool for non-linear data fitting, but the data points in this research are not enough for a satisfactory training result. An innovative interpolation algorithm was developed, it extends the usage of pchip in Matlab to 3-dimensional interpolation, when two variables determine an interpolant. The end result forms a very smooth “surface”. Experiments have shown that the interpolated dew points are very close to the dew points in real measurement, with deviation no more than $\pm 2\text{ }^{\circ}\text{C}$. The industrial standard for empirical humidity sensor deviation is $\pm 3\text{ }^{\circ}\text{C}$. So this algorithm is a very useful tool for humidity sensor temperature compensation. With proper adjustments it can also be used in other property compensation of all kinds of sensors.

8.2 Future Work

As introduced in chapter 2, the humidity measurement is also in close relationship with air pressure. Because this research focuses on sensor temperature compensation and the testing hardware doesn't allow us to test it under different pressures. Although we can get the humidity level under a certain temperature to under different pressures using known conversion formulas. There is a question mark of whether the pressure level has an effect to sensor behavior.

The experiment conditions have great space of improvement, a flat mirror hygrometer is really essential in calibrating this sensor. Also the tubing should be replaced with those made of stainless steel, which suffered much less hydroscopic than hard plastic materials. This makes low humidity measurement more accurate, and the hysteresis phenomenon can be reduced. More advanced testing equipment can also be used in the future that provide greater temperature range and generate a more precise controlled and wider level of ambient humidity. The hardware and software need maintenance and can also be updated for better performance and functionality. The algorithms and techniques in modeling the humidity sensor for temperature compensation can also be utilized for compensation of other properties as well. An automated calibration system can be developed based on those previous researches. It should have the ability to calibrate quite a few humidity sensors simultaneously, record the data and control the air flow rate, humidity level, everything works automatically and need very little human operation.

REFERENCE

- [1] *Water Vapor Measurement: Methods and Instrumentation*, Pieter R. Wiederhold, ISBN-13: 978-0824793197, CRC Press; Har/Dskt edition (April 11, 1997)
- [2] *CRC Handbook of Chemistry and Physics*, CRC Press, London, 76th Edition, ISBN 0-8493-0476-8.
- [3] Kaye and Laby, *Tables of Physical and Chemical Constants*, 16th Edition, Harlow: Longman, ISBN 0-582-22629-5.
- [4] F.C.Quin, The Most Common Problem of Moisture Measurement and Control, *Proceedings of the 1985 International Symposium on Moisture and Humidity*, Washington, D.C.
- [5] General Eastern Instruments, *Humidity Handbook*, Doc, No. A 40103384, Rev B.00, May 1993.
- [6] *ASHRAE Handbook-Fundamentals*, American Society of Heating, Refrigeration and Air Conditioning Engineering, 1993.
- [7] *Method for Measurement of Moist Properties*, ANSI/ASHRAE 41.6-1994, American Society of Heating, Refrigeration and Air Conditioning Engineers, Inc., 1994.
- [8] *A guide to Measurement of Humidity*, ISBN0-904457-24-91, The Institute of Measurement and Control and NPL(UK), 1996.
- [9] Z. Chen and C. Lu, Humidity Sensors: A Review of Materials and Mechanisms, *Sensor Letters*, vol. 3, no. 4, pp. 274–295, 2005.
- [10] L. G. Wade, Jr., *Organic Chemistry*, Prentice Hall, NJ (2001).
- [11] Y. Sakai, Y. Sadaoka, and M. Matsuguchi, *Sens. Actuators B* 35, 85 (1996).
- [12] K. Ogura, H. Shiigi, and M. Nakayama, *J. Electrochem. Soc.* 143, 2925 (1996).
- [13] M. Yang, Y. Li, X. Zhan, and M. Ling, *J. Appl. Polym. Sci.* 74, 2010 (1999).
- [14] F. Ansbacher and A. C. Jason, *Nature* 24, 177 (1953).
- [15] J. M. Thorp, *Trans. Faraday Soc.* 55, 442 (1959).
- [16] S. Chakraborty, K. Nemoto, K. Hara, and P. T. Lai, *Smart Mater. Structure* 8, 274 (1999).
- [17] S. I. Shah, C. P. Huang, J. G. Chen, D. Doren, and M. Barteau, in *Semiconductor metal oxide nanoparticles for visible light photocatalysis. NSF Nanoscale Science and Engineering Grantees Conference*, Arlington, V A (2003).
- [18] S. A. Krutovertsev, A. E. Tarasova, L. S. Krutovertseva, and A. V. Zorin, *Sens. Actuators A* 62, 582 (1997).
- [19] J. Lin, M. Heurich, and E. Obermeier, *Sens. Actuators B* 13, 104 (1993).
- [20] M. d'Apuzzo, A. Aronne, S. Esposito, and P. Pernice, *J. Sol–Gel Sci. Technol.* 17, 247 (2000).
- [21] L. B. Kong, L. Y. Zhang, and X. Yao, *J. Mater. Sci. Lett.* 16, 824 (1997).

- [22] J. F. Boyle and K. A. Jones, *J. Electronic Mater.* 6, 717 (1977).
- [23] G. N. Avani and L. Nanis, *Sens. Actuators B* 2, 201 (1981).
- [24] N. Yamazoe, J. Fuchigami, M. Kishikawa, and T. Seiyama, *Surf. Sci.* 86, 335 (1979).
- [25] Y. Shimizu, M. Shimabukuro, H. Arai, and T. Seiyama, *J. Electrochem. Soc.* 136, 1206 (1989).
- [26] M. G. Kovac, D. Chleck, and P. Goodman, *Solid State Technol.* 21, 35 (1978).
- [27] D. Chleck, P. Goodman, and M. G. Kovac, U.S. Patent No. 4,143,177 (1979).
- [28] R. K. Nahar and V. K. Khanna, *Int. J. Electron.* 52, 557 (1982).
- [29] V. K. Khanna and R. K. Nahar, *Sens. Actuators* 5, 187 (1984).
- [30] I. Emmer, Z. Hajek, and P. Repa, *Surf. Sci.* 162, 303 (1985).
- [31] *MSP430 Microcontroller Basics*, John H. Davies, Newnes; 1 edition (August 21, 2008) ISBN-13: 978-0750682763.
- [32] *MSP430F249 Family User's Guide*, Texas Instruments, December 2004–Revised July 2013.
- [33] *Principles of Semiconductor Devices*, Sima Dimitrijević, Oxford University Press; 2 edition (February 14, 2011), ISBN-13: 978-0195388039.
- [34] *Understanding and Eliminating EMI in Microcontroller Applications*, Texas Instruments, Literature Number: SNOA382.
- [35] *A Practical Guide to Splines*, C. de Boor, Springer-Verlag, New York, 1978
- [36] *Monotone Piecewise Cubic Interpolation*, F. N. Fritsch and R. E. Carlson, *SIAM Journal on Numerical Analysis*, 17 (1980), pp. 238-246.
- [37] *Numerical Methods and Software*, D. Kahaner, C. Moler, and S. Nash, Prentice–Hall, Englewood Cliffs, NJ, 1989.

VITA

Author's Name: Jingbo Tong

Education: BS. in Electronics and Information Engineering, Huazhong University of Science and Technology, awarded June 2010.